Horizontal Convective Rolls: Determining the Environmental Conditions Supporting their Existence and Characteristics

TAMMY M. WECKWERTH

Department of Atmospheric Sciences, University of California, Los Angeles, Los Angeles, California, and Advanced Study Program, National Center for Atmospheric Research, Boulder, Colorado*

JAMES W. WILSON

National Center for Atmospheric Research, Boulder, Colorado*

ROGER M. WAKIMOTO

Department of Atmospheric Sciences, University of California, Los Angeles, Los Angeles, California

N. ANDREW CROOK

National Center for Atmospheric Research, Boulder, Colorado*

(Manuscript received 2 January 1996, in final form 29 July 1996)

ABSTRACT

Data from the Convection and Precipitation/Electrification (CaPE) project, as well as results from numerical simulations, are used to study horizontal convective rolls. The environmental conditions necessary for sustaining rolls and for influencing the aspect ratio, ratio of roll wavelength to convective boundary layer (CBL) depth, and orientation are examined. Observations and numerical model simulations both suggest that a moderate surface sensible heat flux and some vertical wind shear are necessary for roll existence. Unlike some previous studies, however, it is shown that rolls occurred within very low CBL shear conditions ($\sim 2 \times 10^{-3}$ s^{-1}). In addition, the low-level (i.e., $\sim$200 m) shear seems to be more important than the shear through the depth of the CBL in roll sustenance. The aspect ratio is shown to be proportional to the CBL instability, measured in terms of the Monin–Obukhov length. The roll orientation is similar to the wind direction at 10 m AGL, the CBL wind direction, the inversion-level wind direction, and the CBL shear direction. This is not surprising since there was very little directional shear observed within the CBL during CaPE.

1. Introduction

Many studies of horizontal convective rolls (hereafter referred to as rolls), shown schematically in Fig. 1, have been conducted utilizing observations (e.g., LeMone 1973; Kristovich 1993), numerical models (e.g., Sommeria and LeMone 1978; Sykes and Henn 1989; Moeng and Sullivan 1994), laboratory experiments (e.g., Faller 1963, 1965), and theory (e.g., Lilly 1966; Asai 1970a,b, 1972). The majority of the studies (summarized in Table 1) have shown that some combination of surface-layer heat flux and wind shear are necessary for roll existence. The roll wavelength is typically scaled by the boundary layer depth and the orientation of the roll axes is typically along the mean CBL wind and/or shear directions.

A general difficulty with observational studies has been the lack of a direct means to observe and objectively classify rolls. Some researchers defined roll occurrences based on the existence of cloud streets or linear bands of steam fog or haze (e.g., Kuettner 1959, 1971; Angell et al. 1968; Walter and Overland 1984; Brümmer 1985; Miura 1986). When the conditions were not conducive for clouds, fog, or haze to form, this method would not have identified the existence of roll circulations. The presence of linear soaring by seagulls was used to infer roll circulations by Woodcock (1942). Grossman (1982) examined the vertical velocity perturbation of low-level aircraft flights to determine if rolls existed. LeMone (1973) utilized data obtained from four towers to define roll occurrences. Several studies used radar data to examine rolls although they did not include an objective method of defining roll occurrences (e.g.,

* The National Center for Atmospheric Research is partially sponsored by the National Science Foundation.

Corresponding author address: Dr. Tammy M. Weckwerth, NCAR/Advanced Study Program, P.O. Box 3000, Boulder, CO 80307-3000. E-mail: tammy@ucar.edu

© 1997 American Meteorological Society

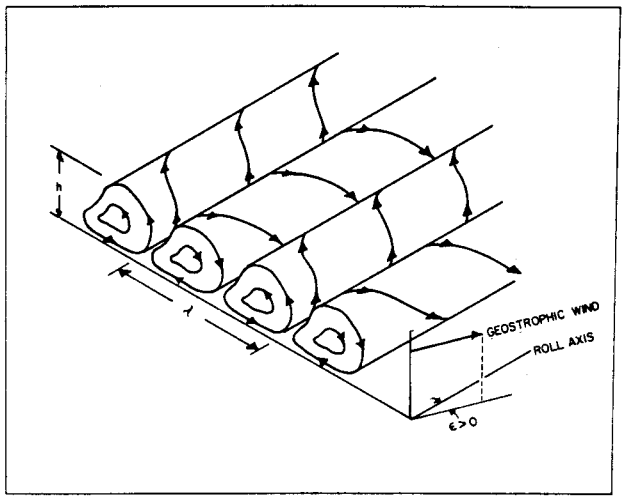

FIG. 1. Schematic diagram of horizontal convective rolls (Brown 1980; Kelly 1982).

Kelly 1982, 1984; Kristovich 1993). Steps are taken in this study to partially overcome some of these earlier difficulties in objectively determining the presence of rolls.

Previous observational studies have typically had only one or two observational platforms to sample rolls and the environmental conditions in which they exist (see Table 1). This has made it difficult to detect rolls and to measure all of the relevant environmental parameters. In addition, Table 1 indicates that most prior studies have had very few cases of roll observations, therefore the generality of the results could not be addressed. Furthermore, the majority of previous studies did not utilize nonroll examples to contrast with the roll occurrences (e.g., LeMone 1973; Christian 1987; Kristovich 1993). Thus, this study was undertaken to utilize an extensive dataset with numerous useful observational platforms to examine a large number of roll and nonroll cases.

The objective of this study is to define the environmental parameters that are conducive to rolls and that define their wavelength and orientation. This research provides a unique addition to the previous work in that it includes the following:

- an objective definition of rolls utilizing radar reflectivity data,
- a comprehensive dataset using several observational platforms,
- numerous roll and nonroll observations, which were obtained in the same location under somewhat varying environmental conditions, and
- an examination of the generality of the results using a three-dimensional numerical model.

The next section presents a review of the previous work. Section 3 provides an objective definition of rolls along with the methodology of the observations and simulations. The procedure for selecting cases is discussed in section 4. Results showing the necessary conditions for rolls are presented in section 5 while the factors influencing their characteristics are shown in section 6. Section 7 includes a summary and a discussion of future work.

2. Background

a. Necessary conditions for roll occurrences

The theories describing the instabilities that lead to rolls may be grouped into two categories: thermal instability and dynamic instability. As summarized in Table 1 many researchers have attempted to show that one or the other instability dominates when rolls occur, however, some combination of the two often exists when rolls are observed.

With thermal instability forcing the rolls, roll energy is obtained from buoyancy while the shear acts to organize the convection into along-shear bands so that the suppressing effect of shear is minimized (Kuo 1963; Asai 1970a,b, 1972). Many studies have indicated that there must be a modest surface heat flux during roll occurrences. The CBL stability, measured in terms of the Monin–Obukhov length, may be slightly stable to very unstable (Christian and Wakimoto 1989; Ferrare et al. 1991) but rolls are most commonly observed within slightly unstable environments (e.g., Grossman 1982; Rabin et al. 1982; Walter and Overland 1984). As the CBL becomes more unstable it is generally expected that growth of two-dimensional convective instabilities is less preferred (e.g., Grossman 1982).

Dynamic instability includes parallel instability (e.g., Faller 1963; Lilly 1966) and inflection point instability (e.g., Brown 1972, 1980; Faller 1965). With parallel instability as the primary forcing mechanism, the roll energy is obtained from the along-roll shear component. Theory suggests that parallel instability will occur only within a neutral environment when the Reynolds number (Re) is small (Lilly 1966). Since Re is generally large in the atmosphere (Brown 1980) parallel instability is likely of secondary importance in the production of rolls. For inflection point instability to be the cause of rolls, the mean large-scale wind profile should have an inflection point in the *cross*-roll direction. This is a dynamic instability in which the rolls grow by extracting kinetic energy from the wind normal to the roll axes (e.g., Stensrud and Shirer 1988; Brümmer 1985).

A few observational studies have suggested that some dynamical criterion must be achieved before two-dimensional organization occurs (e.g., Woodcock 1942; Malkus and Riehl 1964). Christian (1987) observed a minimum CBL wind speed of 5 m s^{-1}. Lidar (Ferrare et al. 1991), tower, and aircraft observations (Wilczak and Businger 1983) showed, however, that rolls could occur with very light ambient winds (less than 2 and 3.5 m s^{-1}, respectively). Miura (1986) observed rolls

TABLE 1. Summary of selected past roll research giving the reference and approach where DDR is dual-Doppler radar, Ac is aircraft, Tow is tower, Sndg is soundings, Sfc st is surface stations, Sat is satellite, Pho is cloud photography, and LES model is large eddy simulation modeling. Also listed are the conditions, where COA is cold-air outbreak, ClA is clear-air, LE is lake-effect snowstorm, and location, where cstl is coastal, ocn is oceanic, L. MI is Lake Michigan, and the remainder locations are the common abbreviations for states' names and the number of cases used. The fourth and fifth columns state whether the cause was related to thermal instability (TI) or dynamic instability [DI; subsets of which are inflection-point instability (IPI) and parallel instability (PI)]. Yes is represented by Y if DI was apparent but the particular type was unknown. No is represented by N. Also listed are whether the previously suggested necessary conditions, as discussed in the text, were met. Dashes imply that the criterion was not examined.

Reference	Approach	Cond. & loc.—No. of cases	TI	DI	$0 < -z_i/L < 21$ (Grossman 1982)	Wind > 5 m s^{-1} (Christian 1987)	Shear $> 10^{-3}$–10^{-2} s^{-1} (Miura 1986)	sh grad $> 10^{-5}$ m^{-1} s^{-1} (Kuettner 1971)
Asai (1970a,b)	Theory	—	Y	Y	—	—	—	—
Atlas et al. (1986)	Lidar, Ac	CAO cstl—1	Y	IPI	—	Y	Y	—
Berger & Doviak (1979)	Radar	ClA OK—1	—	—	Y	Y	—	—
Brown (1980)	Theory	—	Y	IPI	—	—	—	—
Brümmer (1985)	Ac	ClA ocn—3	Y	IPI	Y	Y	—	—
Christian & Wakimoto (1989)	Radar, Pho, Sfc st, Sndg	ClA CO—1	—	—	N; 272	Y	Y	Y
Deardorff (1972)	3D model	—	Y	N	Y	—	—	—
Doviak and Berger (1980)	DDR, Tow	ClA OK—1	Y	IPI	—	Y	—	—
Faller (1965)	Lab	—	Y	—	—	Y	—	—
Ferrare et al. (1991)	Lidar	ClA OK—1	—	Y	N; 250	N; <2 m s^{-1}	—	—
Grossman (1982)	Ac	ClA ocn—4	Y	—	Y	—	—	—
Hildebrand (1980)	DDR	OK—1	—	Y	—	Y	—	—
Kelly (1984)	Radar, Ac	CAO L. MI—3	Y	Y	—	Y	—	—
Kristovich (1993)	Radar, Ac	LE L. MI—4	Y	Y	N; >136	Y	Y	Y; below $0.2z_i$
Kuettner (1971)	Pho, Theory	ClA—5	Y	Y	—	Y	Y	Y
LeMone (1973)	Ac, Tow	ClA—8	Y	IPI	Y	Y	—	—
Lilly (1966)	Theory	—	N	PI	—	Y	—	—
Mason & Sykes (1982)	2D model	—	—	N	Y	Y	—	—
Melfi et al. (1985)	Lidar	CAO ocn—1	—	—	Y	Y	—	—
Miura (1986)	Sat, Sndg	CAO ocn—61	Y	IPI	Y	Y	Y	N
Moeng & Sullivan (1994)	LES model	—	Y	Y	Y	Y	Y	N
Rabin et al. (1982)	DDR, Tow	ClA OK—1	—	—	Y	Y	—	—
Reinking et al. (1981)	DDR, Ac	ClA OK—1	—	—	Y	Y	—	—
Shirer (1986)	3D model	—	Y	PI	Y	—	—	—
Sykes & Henn (1989)	LES model	—	Y	Y	Y	—	Y	—
Walter & Overland (1984)	Sat, Ac	COA ocn—1	Y	IPI	Y	Y	Y	—
Current study	Radar, Sat, Sndg, Pho, Sfc st, Ac 3D model	ClA FL—100	Y	Y	Y	Y	N	N

when the vertical wind shear from 1000 mb to the inversion base was between 10^{-3} and 10^{-2} s^{-1}. Three-dimensional large eddy simulations also showed that increasing the speed shear caused the boundary-layer motions to transform from three-dimensional cellular to two-dimensional linear convection (Sykes and Henn 1989). This is consistent with the theoretical studies of Asai (1970a,b, 1972). Kuettner (1959) observed a curved unidirectional vertical wind shear profile with a maximum wind speed within the CBL when rolls were apparent. He observed that the vertical wind shear gradient ($\partial^2 u/\partial z^2$) was greater than 10^{-5} m^{-1} s^{-1} throughout the CBL when rolls occurred over the Atlantic Ocean. Kristovich (1993) observed lake-effect rolls only when this condition was met within the lowest 200 m of the CBL.

Many theories of roll formation involve a combination of thermal and dynamic instabilities. Deardorff (1972) used the Monin–Obukhov length L, which combines the two instabilities, to predict the onset of rolls. A definition of the Monin–Obukhov length, as given by Stull (1988), is

$$L = \frac{-\bar{\theta}_v(\overline{u'w'_s}^2 + \overline{v'w'_s}^2)^{0.75}}{kg\overline{w'\theta'_{v_s}}},$$

where the overbars represent the mean values, the subscripts s represent near-surface values, θ_v is the virtual potential temperature, $u'w'$ and $v'w'$ are the kinematic

momentum fluxes, k is the von Kármán constant, g is gravitational acceleration, and $w'\theta_v'$ is the kinematic buoyancy flux. The absolute value of the Monin–Obukhov length, which is negative in the CBL, is roughly the height at which buoyancy dominates over shear in the production of turbulence. In essence, L is a measure of convective instability: larger (smaller) Monin–Obukhov lengths indicate less (more) convectively unstable boundary layers. With a three-dimensional numerical model, Deardorff (1972) demonstrated that longitudinal rolls will exist within slightly unstable convective boundary layers (i.e., $0 \leq -z_i/L \leq 4.5$, where z_i is the depth of the CBL). Grossman (1982) observationally recorded roll existence within environments of $-z_i/L < 21.4$ and LeMone (1973) observed rolls when $3 \leq -z_i/L \leq 10$. Similarly, Sykes and Henn (1989) simulated rolls only when $u_*/w_* > 0.35$ or equivalently when $-z_i/L < 9.3$. Rolls, however, have been observed with $-z_i/L$ as large as 250 (Christian and Wakimoto 1989; Ferrare et al. 1991; Kristovich 1993), which contradicts many of the previous findings. As will be discussed in section 3 some of these apparent contradictions may be due to the difficulty in objectively defining rolls with previous datasets.

Many of the previous studies had data from only one or two roll cases, thus this study was undertaken to analyze the necessary conditions for rolls utilizing data on several days at one location. The goal was to examine the conditions in which objectively defined rolls occurred in east-central Florida and to compare the results with past work. Sensitivity studies with a three-dimensional cloud model were included to add to the generality of the observational results.

b. Roll characteristics

It is generally thought that the roll wavelength is dependent upon CBL depth. Kuettner (1971) observed and theoretically predicted an aspect ratio (ratio of wavelength to CBL depth) of 2.8. LeMone (1973) observed aspect ratios of 2.2–6.5. It has been both observed and theorized that larger aspect ratios are due to greater thermal instability (Kelly 1984; Kuo 1963). Rolls with larger aspect ratios have also been observationally and analytically attributed to relatively larger vertical wind shear (e.g., Melfi et al. 1985; Asai 1970a). Conversely in a modeling study, Sykes and Henn (1989) noted that lower shears produced larger aspect ratios. Laboratory experiments (Faller 1965) and analytical studies within an unstable or neutral environment (Shirer 1986) suggested that larger aspect ratios correspond with faster wind speeds. It has also been proposed by Clark et al. (1986) that the aspect ratio is affected by a feedback mechanism wherein the CBL convection induces internal gravity waves within the troposphere, which then regulate the roll aspect ratio within the CBL.

Malkus and Riehl (1964) studied time lapse photography of cloud streets from aircraft flights across the Pacific Ocean and determined that the orientation of cloud streets changed along with the CBL wind direction. A theoretical examination of Ekman layer instability predicted roll orientations relative to the geostrophic wind within the capping inversion (Brown 1972). Within a stable boundary layer Brown (1972) predicted that the roll axes may be up to 30° to the left, while for a neutral boundary layer the orientation should be 18° to the left and for an unstable CBL the axes should be aligned with the geostrophic wind within the inversion. Although this theory is difficult to apply to the CBL since the winds typically do not follow the Ekman profile, LeMone (1973) found that these predictions agreed with aircraft observations. Ferrare et al. (1991), however, observed that the rolls were not oriented along the mean CBL wind nor along the geostrophic wind at the top of the CBL but rather within 15° of the CBL wind *shear* direction. Shirer (1980) developed a linear theory to predict roll orientation based upon the CBL wind shear gradient. Kelly (1984) showed good agreement between Shirer's model and observations.

The predictions of previous studies have been tested with the CaPE dataset using an objective method of defining roll wavelength and orientation. The inclusion of the numerical simulations allowed for verifying the results within a larger parameter space than was observed.

3. Definition of convective modes and methodology

The observational dataset was obtained from the CaPE project, which was conducted in east-central Florida during the summer of 1991. The observational network for this study was described by Wakimoto and Atkins (1994). Observations utilized herein were primarily obtained from NCAR's (National Center for Atmospheric Research) CP-3 and CP-4 Doppler radars, CLASS (Cross-chain Loran Atmospheric Sounding System) soundings, PAM II (Portable Automated Mesonet) surface stations, cloud photographs, *GOES-7* visible satellite imagery, and the NCAR and UW (University of Wyoming) King Air research aircraft.

a. Justification for using clear-air radar features

The NCAR radars were the primary platforms used to determine the characteristics of the boundary layer convection in this study. Through comparisons with dual-Doppler analyses, in situ aircraft measurements and cloud locations obtained from photogrammetric techniques, Wilson et al. (1994) showed that clear-air reflectivity fine lines represented updrafts within the CBL. It is unknown, however, if the radar is always capable of identifying convective features. It is likely that in some cases the scale of the convection was too small (i.e., < 1 km) for the radar to resolve the features. The assumption was made that the radar reflectivity dis-

tinguished the convective modes, but it is plausible that there were times that small-scale convection was not detected. Although the radar is not a perfect indicator of convective features, it will be shown in the following section that it is more discriminating to the convective mode than the common alternative of visible satellite imagery.

b. Definition of convective modes

To objectively define rolls and determine their wavelength and orientation, a spatial autocorrelation routine was applied to radar reflectivity data. The first step was to edit the radar scans and remove ground clutter, spurious echoes, and second-trip echoes using the NCAR Research and Data Support System (RDSS) computer software (Oye and Carbone 1981). The radar reflectivity within a 15 km $\times$ 15 km box was interpolated onto a Cartesian grid using the Cressman (1959) interpolation scheme with a grid spacing of 250 m. This domain size was large enough to include several rolls but small enough to assume that the characteristics within the domain were uniform. This gridded reflectivity at approximately $0.7z_i$ was then shifted grid point by grid point in orthogonal horizontal directions and a correlation coefficient was calculated for every shift. This is a pattern recognition technique similar to that performed by Kessler and Russo (1963). The resultant spatial autocorrelation field was contoured with correlation coefficient values of 0.1, 0.2, and 0.3. The 0.2 correlation coefficient contour in the center of the domain was chosen to define the convective mode. A measurement of the contour's major axis versus its minor axis determined the horizontal aspect ratio (HAR). After a visual inspection of many cases, it was decided to use an HAR greater than 6 as a criterion for roll existence. This procedure was not only useful for categorizing the convection but also for measuring an average wavelength and orientation, which were both variable within the radar reflectivity field.

Examples of four radar reflectivity scans corresponding to the four convective modes defined for this study are shown in Fig. 2. At 1700 UTC (hereafter all times will be UTC; UTC = EDT + 4 h) on 6 August 1991, the convection, as observed by the radar, had a well-defined linear structure (Fig. 2a). The interpolated radar reflectivity indicated northwest–southeast linear bands of convection (Fig. 3a) and the spatial autocorrelation field also supported this observation with an HAR of 14.7 at $0.89z_i$ (Fig. 4a). Notice that by using the raw radar reflectivity (Fig. 2a) it was difficult to define a wavelength and orientation since the separation and orientation of fine lines varied. Using the autocorrelation method, however, an average wavelength and orientation over the domain were objectively determined. The wavelength was measured from the center to the center of the correlation coefficient bands (4.3 km in this example), while the orientation was determined from the center 0.2 contour (145°–325° in this example). Note that the orientation is similar to the PAM wind direction (Fig. 2a).

The corresponding visible satellite image at 1700 UTC is shown in Fig. 5. The region in which the autocorrelation routine was performed is indicated by a box. Notice that rolls existed even though cloud streets were not apparent near the analysis region. This is an example showing that if the existence of cloud streets were the only available method to determine whether or not rolls existed, it would have been mistakenly determined that rolls were not occurring due to a lack of cloud streets.

At 2000 on 12 August the radar reflectivity indicated cellular convection (Fig. 2b). The enhanced north–south line of reflectivity was caused by the sea-breeze front and care was always taken to exclude it from the autocorrelation routine. Previous studies of open cells have shown that they are commonly hexagonal in shape (e.g., Rothermel and Agee 1980) but this radar reflectivity field suggested that the fine lines sometimes formed rectangular shapes, as did cellular convection on other days observed during CaPE. The convective features within the box almost appeared as a combination of two transverse linear structures with orientations of northwest–southeast and northeast–southwest. Although the interpolated field did not clearly show a cellular pattern (Fig. 3b), it was again evident in the autocorrelation field (Fig. 4b). The spatial autocorrelation field at $0.65z_i$ produced an HAR of 1.4 and a somewhat northwest–southeast linear structure. There also appeared, however, to be a northeast–southwest organization that was consistent with the PAM wind direction (Fig. 2b). These features (i.e., HAR $<$ 2.0 and two nearly orthogonal organizations) were consistent with other examples of open cells observed during CaPE.

The satellite imagery at 2000 on 12 August did not indicate cellular convection but rather showed some suggestion of cloud streets near the analysis region (Fig. 5). Although cloud streets were evident in satellite imagery over a relatively larger domain, rolls were not apparent when looking at the local radar images. Thus, previous studies may have defined cases as rolls when, in fact, rolls were not actually occurring within a particular local region. This may partially explain why past studies have produced some contradictory results on the necessary environmental conditions for roll occurrences.

The radar reflectivity field at 1830 on 10 August showed somewhat linear convection although there was also a great deal of variability (Fig. 2c). This convective pattern did not meet the criterion for roll convection. The interpolated reflectivity within the box at $0.65z_i$ is shown in Fig. 3c and this produced an HAR of 3.1 (Fig. 4c). There was not a well-defined wavelength although there was a dominant orientation (89°–269°) that was within 20° of the PAM wind direction shown in Fig. 5. This is an example of unorganized convection. Although

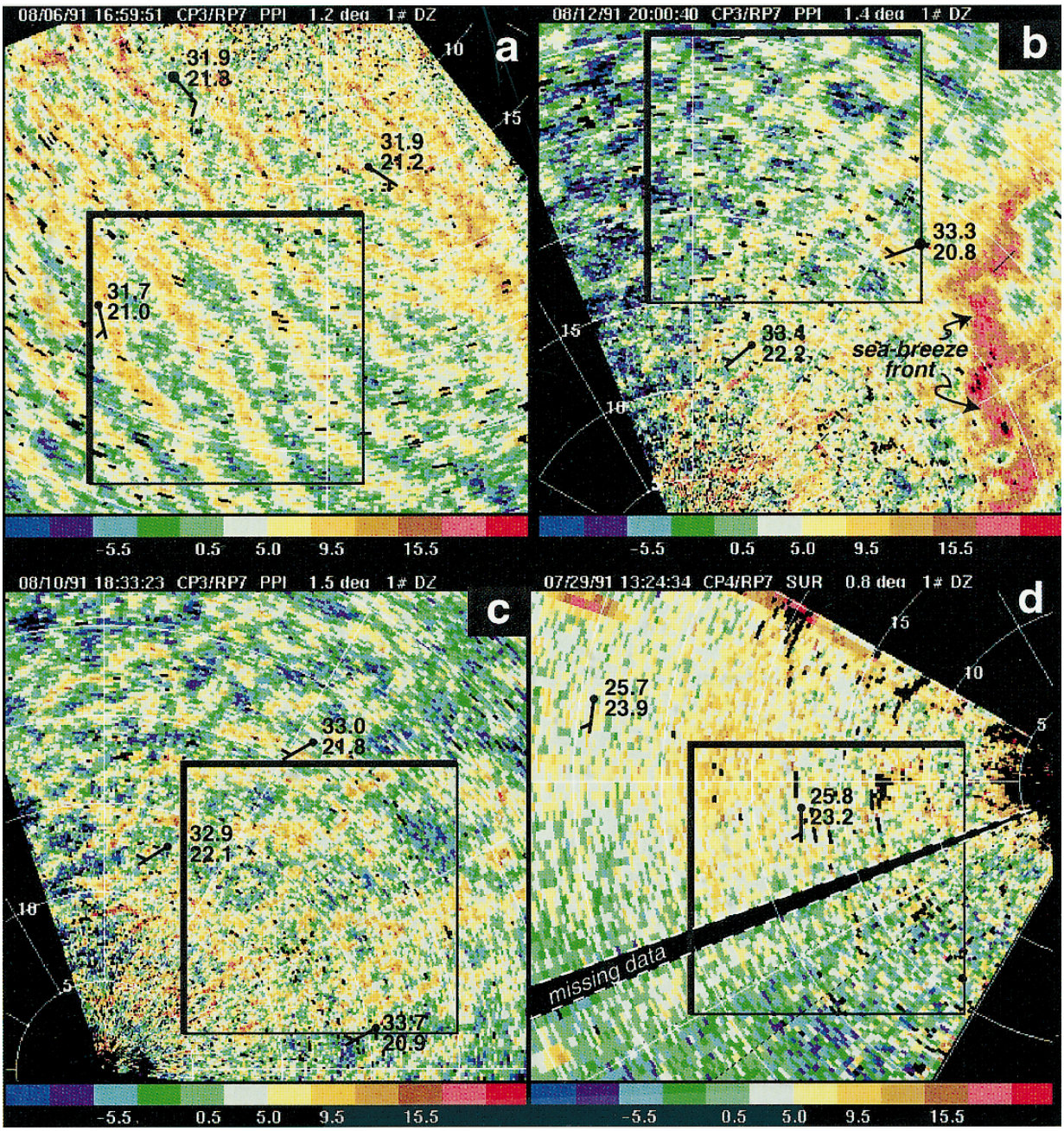

FIG. 2. CP-3 radar reflectivity field at (a) 1700 UTC 6 August 1991, (b) 2000 UTC 12 August 1991, (c) 1830 UTC 10 August 1991, and (d) 1330 UTC 29 July 1991. Select PAM station data points are overlaid supplying temperature (°C; top), dewpoint temperature (°C; bottom), and winds (full barb is 5 m s^{-1}; half-barb is 2.5 m s^{-1}). The boxes indicate the region of interpolated reflectivity shown in Fig. 3.

the criterion for roll convection was not met in this localized area, the satellite imagery once again suggested that cloud streets were occurring near the analysis region at this time (Fig. 5).

The final example at 1330 on 29 July 1991 exhibited no convective features (Fig. 2d). Since rolls typically occurred by 1330, this mode was rarely observed due to the late start-up time during CaPE (i.e., 1330). The radar reflectivity field displayed no apparent convective features at $0.63z_i$ (Fig. 3d). The HAR was nearly 1, similar to that of cellular convection, but there was no structure in the autocorrelation field (Fig. 4d). The satellite imagery showed a lack of clouds over the analysis region. The PAM winds over the peninsula were light and variable (Fig. 5).

A number of sensitivity tests were performed on this

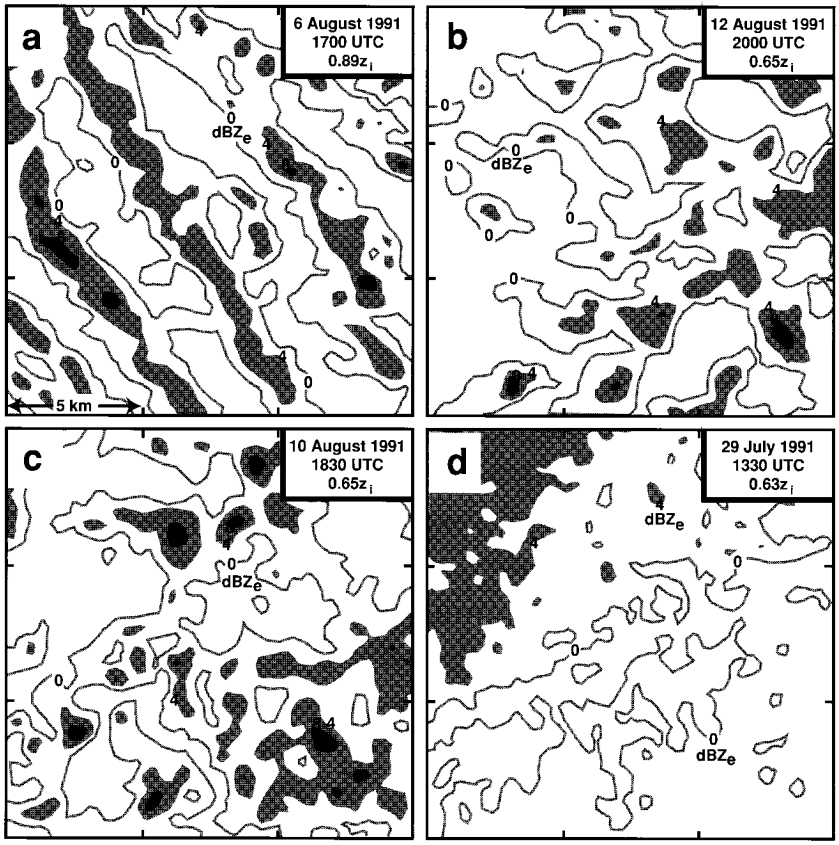

FIG. 3. Interpolated CP-3 radar reflectivity (dBZ_e) from within the boxes of the respective images of Fig. 2. Contours are every 4 dBZ_e starting at 0. Values greater than 4 dBZ_e are lightly shaded and those greater than 8 dBZ_e are darkly shaded. Normalized height at which interpolation was performed is shown in the upper right.

spatial autocorrelation routine to examine its reproducibility. There was little variation in the results when performing the analysis on a series of consecutive times (i.e., at approximately 3-min intervals). Various radii of influence were also used to determine the sensitivity to the gridding scheme. The results did not change noticeably. The spatial autocorrelation routine was, however, sensitive to the radar used. Due to the radar beams sometimes being blocked by trees at low levels, one of the radars often observed the features more clearly than the other radar. The radar with the most unobstructed view of the region of interest, typically CP-3, was chosen for the analysis. The elevation angle closest to 1° was used since this angle showed the rolls most clearly and produced autocorrelation fields that were within the CBL. In addition, the spatial autocorrelation routine was sensitive to the domain analyzed. A domain as near as possible to the location of the data source used for measurements of independent variables (i.e., sounding or radar) was chosen. A weakness in this method was that different results (i.e., different HARs, wavelengths, and orientations) were sometimes obtained when the box was moved. This was due primarily to a departure from horizontal homogeneity in the convective structure, as depicted by the reflectivity fields (apparent in Fig. 2). This may, however, represent real spatial variability in convection.

Note that in these examples, the satellite images corresponding to cellular and unorganized convection suggested the existence of cloud streets, while the case of roll convection did not display cloud streets in the analysis region (Fig. 5). When focusing in on a relatively smaller area with the radar, a pronounced difference in the convective organization was often apparent (e.g., compare the unorganized convection observed with radar of Fig. 2c to the corresponding fairly well-defined cloud streets of Fig. 5). Thus, one reason for some of the contradictions in previous work may be in the definition of rolls based upon the existence of cloud streets.

c. VAD methodology

One of the primary requirements for this study was an accurate measurement of CBL horizontal winds and vertical wind shear. Soundings were of limited usefulness in that they were taken only a few times per day. Also they produced only a vertical profile of point measurements, which did not necessarily correspond with

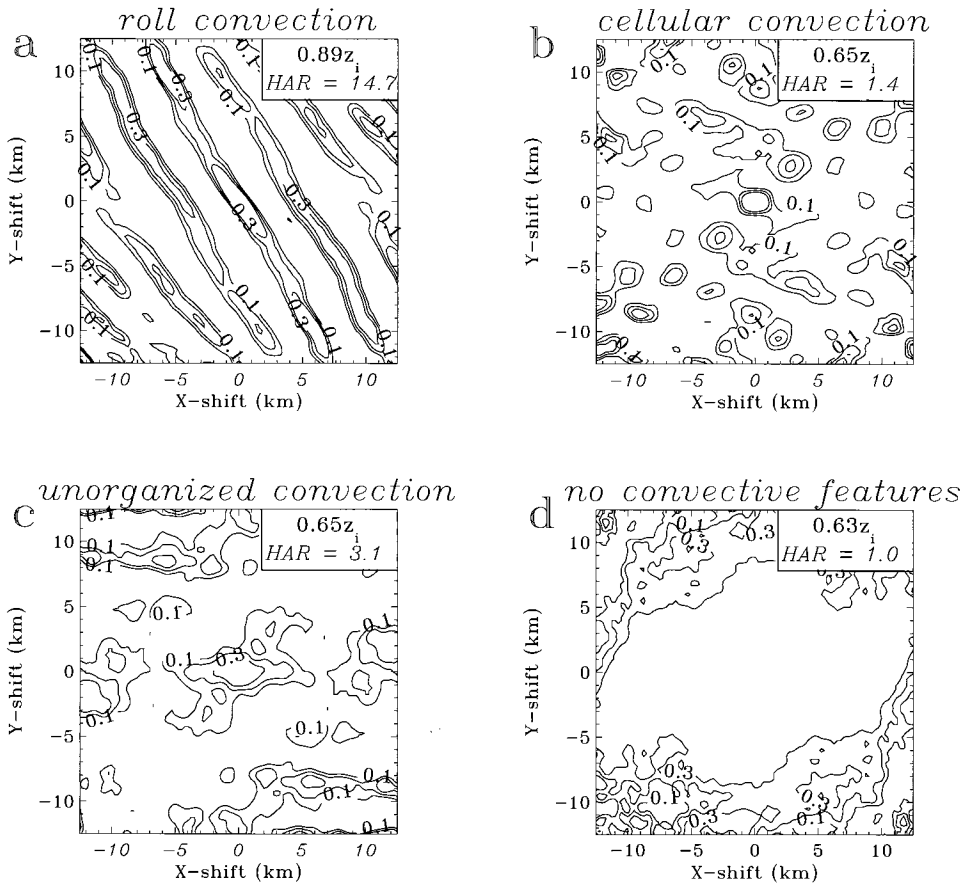

FIG. 4. Spatial autocorrelation fields generated from the domains displayed in Fig. 3, respectively, showing (a) roll convection, (b) cellular convection, (c) unorganized convection, and (d) no convective features. Correlation coefficients of 0.1, 0.2, and 0.3 are contoured. The axes give the associated shifts (km). Normalized heights of the analyses and the resulting HARs are given in the upper right.

the mean wind in the region of roll occurrences. To alleviate this difficulty the velocity–azimuth display (VAD) routine (Matejka and Srivastava 1991) was performed upon CP-3 radar data. The highest elevation angle routinely available (~8°) was used in the VAD analysis. As an example of areal coverage, the VAD retrieval at a height of 2-km utilized data within a 14-km range from the radar, which provided an areal wind profile over several rolls. The analysis technique yielded unrepresentative winds within the lowest 200 m due to contamination by ground clutter and an averaging radius of less than 1.2 km.

d. CBL depth measurements

The depth of the CBL was determined from sounding data when available. The well-mixed layer in potential temperature and mixing ratio was generally easily identified. As with the wind measurements, however, it was often desirable to know the depth of the CBL when a sounding was unavailable. For these times, the radar reflectivity profiles were used. The height at which there was a change in slope of the reflectivity profile was defined as the top of the CBL (Kaimal et al. 1982). Comparisons showed that these measurements were within about 300 m of the sounding CBL depth values with the radar technique typically overestimating the depth (Weckwerth 1995).

e. Three-dimensional Clark cloud model

To address the generality of the results and to examine roll features under widely varying environmental conditions, the Clark cloud model was utilized. The three-dimensional, anelastic, nonhydrostatic, finite-difference model is described in Clark (1977) and Clark and Farley (1984). A dry version of the model was used with the Coriolis force included. The domain size was nominally 18 km × 18 km × 10 km with a horizontal grid spacing of 250 m × 250 m. A vertically stretched grid was used with a grid spacing of 100 m in the lowest 3 km, linearly increasing to a maximum of 400 m above 3 km. An 8-s time step was utilized for 2 h by which time the vertical profiles of all fields had reached a nearly steady state.

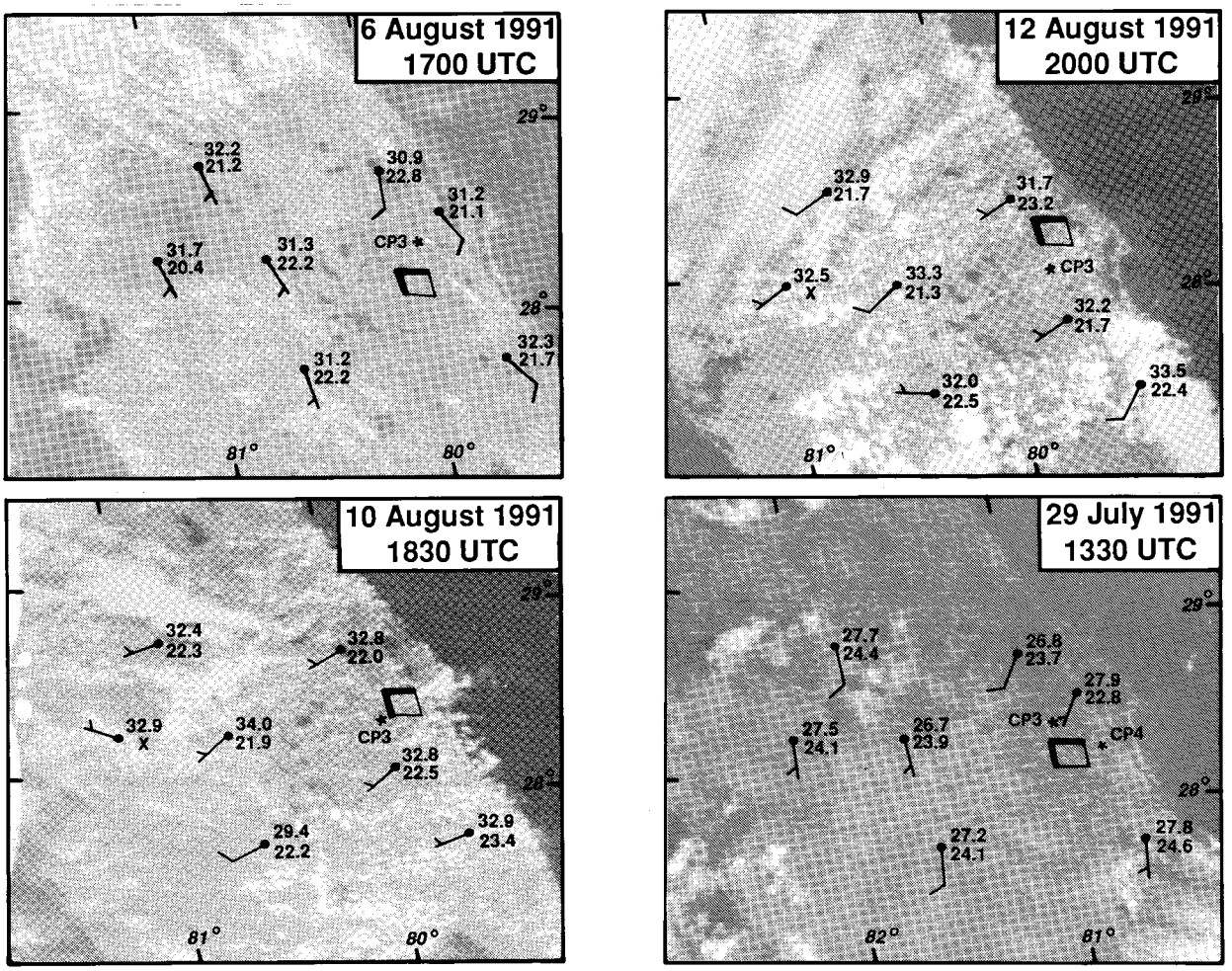

FIG. 5. Visible satellite imagery corresponding with (a) rolls, (b) cellular convection, (c) unorganized convection, and (d) no convective features of Fig. 2. Selected PAM surface station temperature and dewpoint temperatures are plotted along with the winds (full barb is 5 m s^{-1} and a half-barb is 2.5 m s^{-1}). The boxes indicate the areas of interpolated radar reflectivity of Fig. 3 used to categorize the convective features.

Cyclic lateral boundary conditions were applied and a Rayleigh damping layer in the upper third of the domain was utilized to absorb vertically propagating internal gravity waves. The surface sensible heat flux was varied between 25 and 400 W m^{-2}. In the first 20 min of each simulation, a random surface heat flux with a maximum amplitude of 1 W m^{-2} was applied. A potential temperature profile that was similar to the midday CaPE observations was used to initialize all runs. The CBL was dry adiabatic with a potential temperature of 300 K. The simulations were initialized with constant stability aloft defined by a Brunt–Väisälä frequency of 0.012 s^{-1}. Thus, the initial state was horizontally homogeneous and an inhomogeneous evolution occurred owing to the random perturbations on the surface heat flux.

The simulations were initialized with only a meridional component of wind, which was varied between 2 and 15 m s^{-1}. A Galilean transformation was performed to keep instabilities within the domain for longer periods of time. For example, to obtain an effective wind speed of 10 m s^{-1}, the simulation was initialized with a 5 m s^{-1} westerly wind component and the surface was forced to move 5 m s^{-1} to the west. The value of the surface drag coefficient C_D was chosen as 0.2. Although realistic surface drag values are typically an order of magnitude less, this value was necessary to maintain the shear at low levels. Generally, this low-level shear would be maintained by momentum advection and/or a large-scale pressure gradient. Since it is difficult to include these large-scale effects in a limited domain, it was necessary to increase the surface drag to an artificially high value. Hauf and Clark (1989) and Balaji and Clark (1988) discuss this point in further detail.

4. Selection of observational cases

Days with well-defined rolls, as determined by radar and satellite data at 30-min intervals, were first chosen

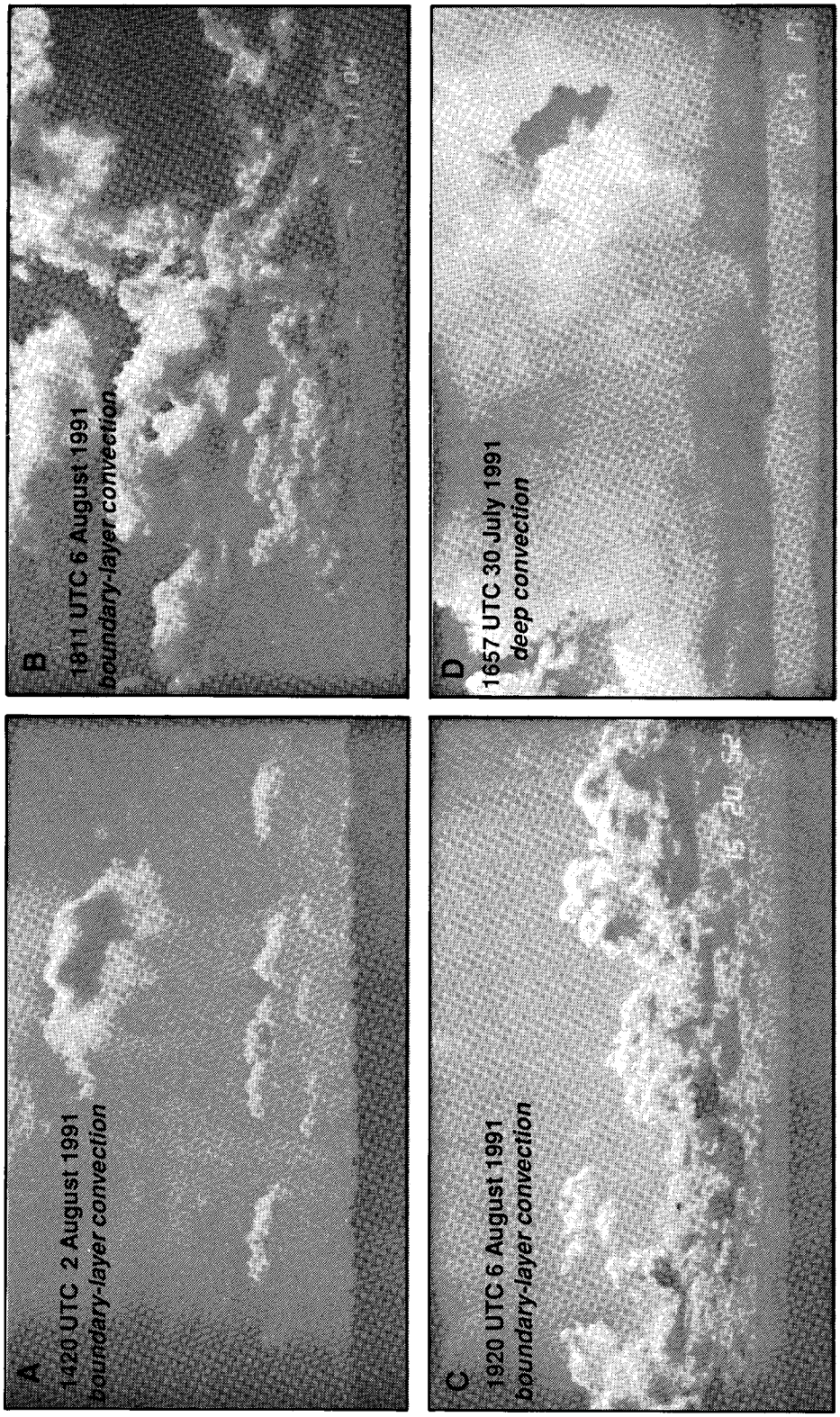

FIG. 6. Examples of cloud photographs used to verify the existence of boundary layer convection. Boundary layer convection was defined for (a), (b), and (c) while (d) included relatively deep convective clouds. Cases such as shown in (d) were eliminated from the analyses.

for analysis. In addition, cases were added for those times when rolls were not well defined. Over 100 cases were examined although not all of these cases were complete. For example, some did not have a surveillance scan necessary for VAD wind analysis while other cases were missing a sounding necessary for temperature measurements. There were 63 complete cases, some of which were discarded after observing deep convection with the photographs and satellite imagery.

Since the focus of this study is boundary-layer rolls, only cases in which shallow or no convective clouds were occurring have been analyzed. During these events, which have been termed boundary layer convection cases, it was assumed that the CBL motions were unaffected by the cloud circulations. Thus, if deep, moist convection was occurring (e.g., towering cumulus), the case was eliminated from the analyses. The cloud photos taken from the CP-3 and CP-4 radar sites were primarily used to categorize the convective development. Although this was accomplished subjectively it was relatively easy to classify the cases in terms of shallow cumulus clouds or deep convection. Satellite imagery was used to confirm the categorizations. Four cloud photo examples are shown in Fig. 6. The first three examples were included within the category of boundary layer convection (Figs. 6a, 6b, and 6c) while at 1700 on 30 July (Fig. 6d) there was relatively deep, moist convection. Thus, the latter case was eliminated from the analyses. This elimination of deep convection cases resulted in a total of 45 complete cases, 13 of which were roll cases.

5. Environmental conditions sustaining rolls

a. Thermodynamics of the environment

It is desirable to be able to predict whether boundary layer convection will occur, and if so, in what form. It has long been known that the onset of convection is determined by the Rayleigh number reaching a critical value (Rayleigh 1916). One of the primary variables in the Rayleigh number when applied to the atmosphere is the virtual potential temperature difference across the depth of the CBL. Measured in terms of the virtual potential temperature, there was little variation in the Florida CBL stability profiles for the cases analyzed (not shown).

Another estimate of thermal stability may be obtained from the surface sensible heat flux. Since heat flux measurements were not available during CaPE, an estimate was obtained by calculating $U\Delta T$ (Stull 1988) where U is the PAM II wind speed at 10 m and ΔT is the PAM II temperature at 2 m minus the soil temperature. Figure 7 shows some indication that the five cases with no convective features apparent in the radar data were less unstable (i.e., less negative values) than the rest of the cases. The cellular convection occurred within a narrow range of sensible heat flux values while the roll cases encompassed a broader, yet limited, range. The unorganized convection data points extended throughout the entire range of measurements. Some of the HAR measurements were obtained from radar scans of the south dual-Doppler lobe while all of the $U\Delta T$ measurements were obtained from the north dual-Doppler lobe, so it was necessary to assume that neither the HARs nor $U\Delta T$ varied significantly in space.

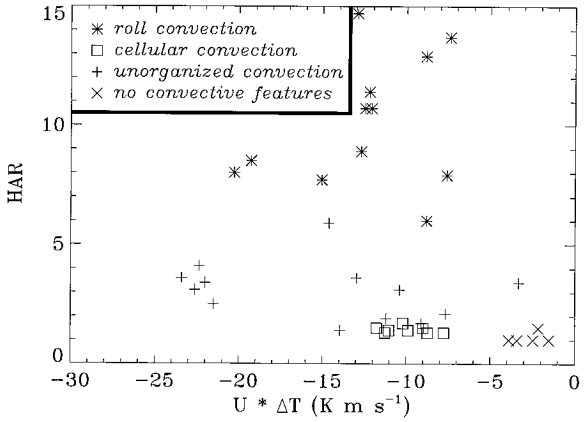

FIG. 7. Sensible heat flux (K m s^{-1}) vs HAR. Data points are partitioned into the four radar-determined convective modes.

Simulations with the Clark cloud model did not suggest a minimum but did suggest a maximum heat flux above which rolls were not well defined. Figure 8 shows a comparison between three runs with different sensible heat flux input parameters. The left column shows the potential temperature and velocity profiles at 2 h of simulation time. The right column displays the corresponding spatial autocorrelation field calculated for the vertical velocity field. Lower correlation coefficient values were obtained, as compared with the observations, thus only qualitative comparisons were made. This may have been due to the use of instantaneous vertical velocity in the simulations while the reflectivity field, which responds to the time-integrated vertical velocity, was used in the observations. The run with a sensible heat flux of 25 W m^{-2} ($-z_i/L = 5.6$) was most similar to observations at midday when the rolls were typically well defined. This simulation produced roll-like convection (Fig. 8b). The run with a sensible heat flux of 200 W m^{-2} ($-z_i/L = 56.7$) most likely corresponded to conditions in the afternoon. Indeed Fig. 8d suggests that well-defined rolls were occurring for this simulation. Although all of the simulations suggested that there was some linear convection, the simulation with a sensible heat flux of 400 W m^{-2} produced less-organized convective features (Fig. 8f). This was as expected due to its large $-z_i/L$ ratio (129.4).

Just as much of the theoretical and laboratory work previously showed, the stability of the environment aided in the determination of whether or not convection was expected to occur. Not only did the surface-layer heat flux seem to determine if thermal convection would occur but there was a suggestion that the roll convection

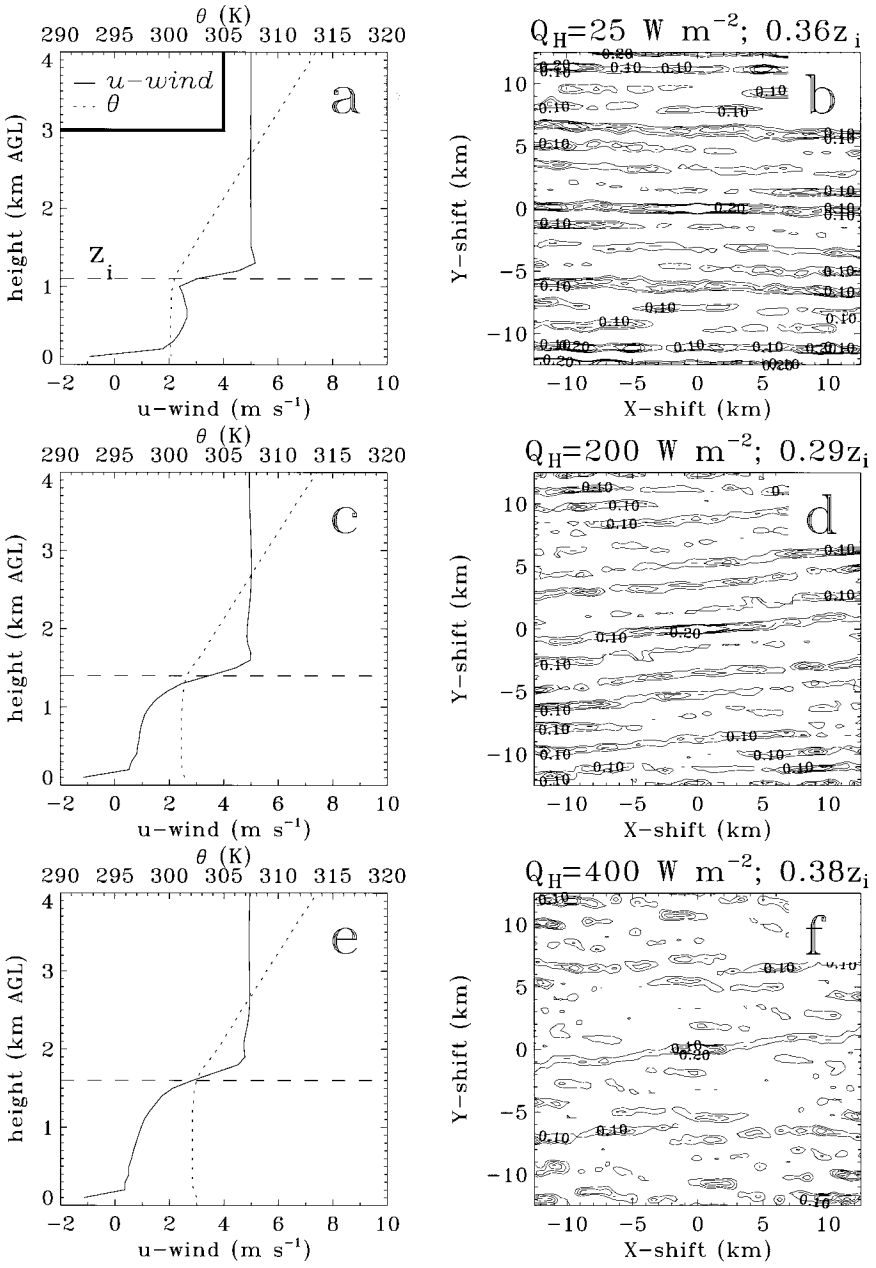

FIG. 8. Model output at 120 min comparing various sensible heat flux input parameters: (a,b) 25 W m^{-2}, (c,d) 200 W m^{-2}, and (e,f) 400 W m^{-2}. The left column shows the potential temperature (K; dashed line) and meridional wind component (m s^{-1}; solid line) profiles. The top of the CBL is indicated by the horizontal dashed line. The right column shows the corresponding results from the autocorrelation routine performed upon the vertical velocity field. The height at which the routine was performed is indicated at the top of (b), (d), and (f).

occurred within a certain range of sensible heat fluxes. The numerical simulations also implied a cutoff value of surface sensible heat fluxes above which rolls were less well organized.

b. Dynamics of the environment

Perhaps the most generally accepted theory governing which type of convective mode will exist when the Rayleigh number reaches its critical value is based upon the magnitude of the CBL vertical wind shear. Theory predicts that the main parameter governing whether convection will be two- or three-dimensional is the value of the shear: for low shears, the convection should be cellular while higher shears should allow for the existence of rolls (e.g., Asai 1970b). Figure 9 basically shows similar results; that is all cases of open cells

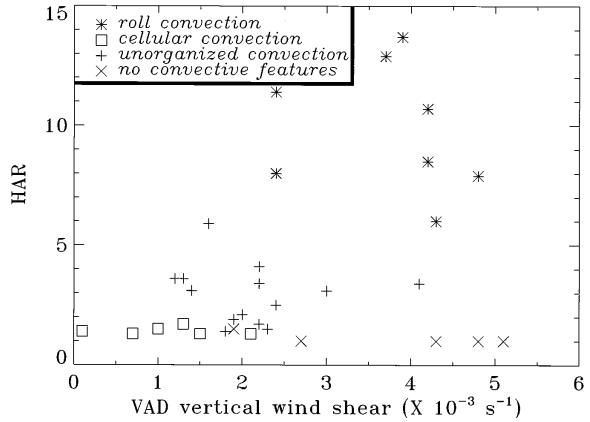

FIG. 9. CBL vertical wind shear ($\times 10^{-3}$ s^{-1}) vs HAR. Data points are partitioned into the four radar-determined convective modes.

existed when the CBL vertical wind shear (calculated using the wind at the top of the CBL and the 10-m PAM wind) was less than approximately 2×10^{-3} s^{-1} while rolls occurred when the shear was larger. The value of 2×10^{-3} s^{-1}, however, is quite low compared to the results of some previous studies (e.g., Miura 1986).

The CBL shear was typically small during CaPE (i.e., $2–8 \times 10^{-3}$ s^{-1}). Figure 10 shows a time series of VAD wind profiles. The lowest 200 m of the VAD profiles are not plotted due to inaccurate retrieval at low levels. When available, the sounding winds were also plotted in Fig. 10. Note that there was virtually no directional shear up to the maximum retrievable height. Wind speeds throughout the CBL did become more well mixed as the day progressed, leading to lower shear values.

Some of the previous observational studies have suggested that there is a minimum wind speed criterion that must be met before rolls can exist (e.g., Woodcock 1942; Malkus and Riehl 1964). The data from Florida also suggest that there was a sharp increase in the radar-determined HAR above a mean CBL wind speed threshold of approximately 5.5 m s^{-1} (Fig. 11). The PAM 10-m wind speed threshold for rolls was 3 m s^{-1} (Fig. 12). The cellular and no convective feature cases occurred with relatively lower mean CBL and 10-m wind speeds, while the unorganized convective events encompassed a range of wind speeds.

Sensitivity tests with various magnitudes of wind speed were performed with the model. Qualitatively the simulated results were similar to the observations. The first simulation with an effective wind speed of 2 m s^{-1} (Fig. 13a) produced unorganized convection (Fig. 13b) and had a high $-z_i/L$ ratio (696). When the wind speed was increased to 5 m s^{-1} (Fig. 13c) and 10 m s^{-1} (Fig. 13e), however, linear convection was produced (Figs. 13d and 13f) with respective $-z_i/L$ values of 44 and 6. This result showing that rolls do not exist for low wind speeds is consistent with the CaPE observations.

There have been various theories proposed suggesting that some other measurement of wind will aid in predicting when convection will become two-dimensional. Brown's (1970, 1972) theory predicts that rolls will exist when there is an inflection point in the cross-roll wind speed profile (i.e., a point at which the curvature of the cross-roll wind speed profile changes sign). Results of testing this hypothesis with the CaPE dataset were inconclusive (not shown). There were not always inflection points when rolls were observed and there was one case in which open cells were observed with an inflection point profile. This linear theory, however, is difficult to verify observationally since the rolls act to eliminate the inflection point once they have formed.

Kuettner (1971) found a minimum criterion in the curvature of the wind speed profile (i.e., change in wind shear with height) for rolls observed over the tropical Atlantic Ocean. He determined that this value was $10^{-7}–10^{-6}$ cm^{-1} s^{-1} with a curved unidirectional velocity profile in which the wind speed reached a maximum somewhere within the CBL. Although this profile did sometimes occur during roll events, it was not present during all CaPE roll events (see profiles in Fig. 10 corresponding to roll occurrences from 1500 to 1600).

In summary, as noted in some of the previous work, these results suggest that a minimum mean CBL (10 m) wind speed criterion of about 5.5 m s^{-1} (3 m s^{-1}) be met before rolls occur in east-central Florida. The minimum wind speed criterion was also verified in the numerical simulations. In addition as theory predicted, three-dimensional cellular convection existed within low shear environments while two-dimensional rolls occurred during relatively higher CBL shear conditions. The threshold, however, was only about 2×10^{-3} s^{-1}, which is not a difficult value to achieve and is lower than that previously thought necessary to sustain rolls.

c. Thermodynamics and dynamics of the environment

The two previous sections have suggested that both thermodynamics and dynamics play a role in determining when rolls exist. This has also been noted by previous investigators. The combination of thermodynamics and dynamics is shown in Figs. 14 and 15. The observed cases were partitioned into different categories based upon the radar-determined convective modes. Figure 14 suggests that some combination of sensible heat flux and wind shear influenced the convective mode. The cases with no convective features occurred with a variety of wind shear values but within low heat flux environments. The rolls existed within only a certain range of $U\Delta T$ values when the wind shear across the CBL was greater than 2×10^{-3} s^{-1}. The apparent factor distinguishing between cellular and roll convection was the magnitude of the shear, as predicted by Asai (1970b).

Similar results were observed when plotting $U\Delta T$ versus mean CBL wind speed (not shown) and PAM wind speed (Fig. 15). These results are similar to Woodcock's (1942) observations of sea gulls soaring over the ocean.

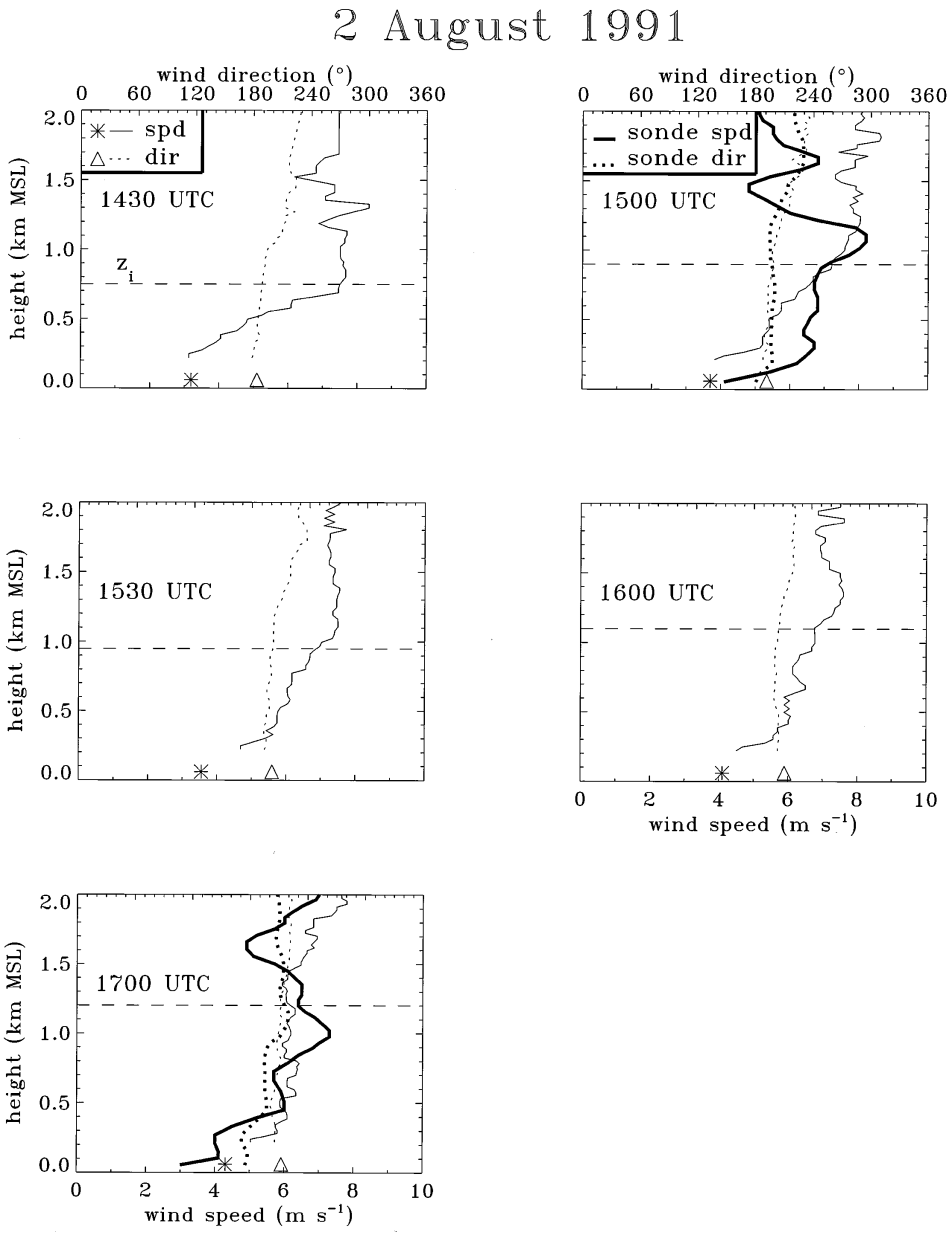

FIG. 10. Time series of VAD wind speed (m s^{-1}; solid lines) and direction (°; dotted lines) profiles on 2 August 1991. The surface points are PAM wind speeds and directions. When available (1500 and 1700 UTC), sounding winds were overlaid using thick lines and dots. The top of the CBL is indicated by a dashed horizontal line.

He noted that their soaring patterns were linear (i.e., indicative of roll convection) only when the winds were relatively high and the surface sensible heat flux (for which he used ΔT as a proxy) was a moderate value.

Using surface-layer similarity theory and some simplifications, the measured parameters were converted into a proxy for $-z_i/L$, termed Z (e.g., Stull 1988):

$$-\frac{z_i}{L} \sim Z \equiv \frac{z_i k g \Delta T}{T U^2},$$

where T is the PAM temperature at 2 m, U is the PAM wind speed at 10 m, and all other parameters are as previously defined. This relationship assumes that the exchange coefficients for heat and momentum are identical. This is not necessarily true since the heights at which the measurements were taken were not the same. Thus, the absolute magnitudes of Z are not known with certainty but the relative magnitudes are believed to be accurate. Results of calculating Z for this dataset are shown in Fig. 16. Note that all of the roll cases occurred

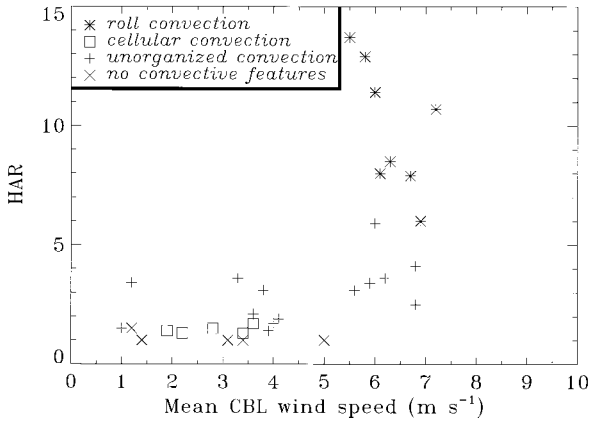

FIG. 11. Mean CBL wind speed (m s^{-1}) vs HAR. Data points are partitioned into the four radar-determined convective modes.

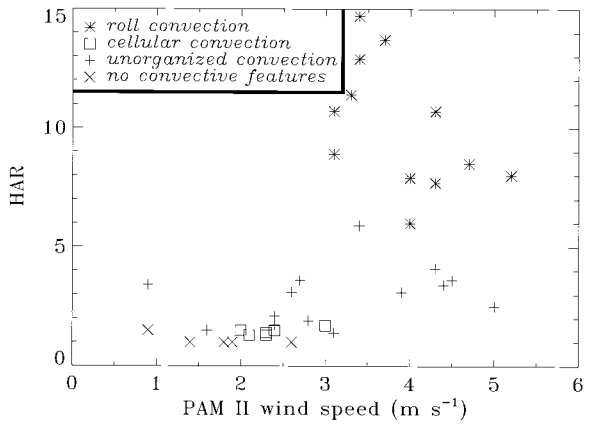

FIG. 12. PAM II wind speed at 10 m (m s^{-1}) vs HAR. Data points are partitioned into the four radar-determined convective modes.

within less unstable (low Z values) environments than the cellular convection cases. This result is similar to that of Grossman (1982) and LeMone (1973).

In an attempt to determine the dominant instability forcing the rolls, the primary roll-forcing mechanisms were calculated in a manner similar to that of LeMone (1973), who examined the terms of the turbulent kinetic energy (TKE) budget given by

$$\frac{\partial}{\partial t}\bar{E}' = \frac{g}{\bar{\theta}_v}\overline{\theta_v' w'} - \overline{u'w'}\frac{d}{dz}\bar{U} - \overline{v'w'}\frac{d}{dz}\bar{V} - D,$$

(B) (SA) (SC)

where the primes denote the perturbation quantities due to the rolls, the overbars denote the spatially averaged means, $\bar{\theta}_v$ is the mean virtual potential temperature, $\overline{\theta_v' w'}$ is the mean thermodynamic flux, $\overline{u'w'}$ is the mean along-roll momentum flux, $\overline{v'w'}$ is the mean cross-roll momentum flux, and D is the loss due to viscous dissipation. The first term on the right denotes the production of energy by buoyancy (B) and represents roll forcing by thermal instability, and the second and third terms denote the production of roll kinetic energy by the along-roll (SA) and cross-roll wind shear (SC) components. In this study the SA and SC terms were combined to represent roll forcing due to a generic shear instability (S).

The vertical velocity data from the UW King Air were corrected for known biases obtained from intercomparison flights with the NCAR King Air and tower fly-bys, as done in Fankhauser et al. (1985). This correction required a subtraction of 0.3 m s^{-1} for the UW King Air vertical velocity measurements. The expected absolute accuracies (precisions) of the aircraft potential temperature and vertical and horizontal velocities were 0.4 K (0.04 K), 0.2 m s^{-1} (0.05 m s^{-1}), and 1.0 m s^{-1} (0.05 m s^{-1}), respectively (Kessinger 1988). The buoyancy (B) and shear (S) production terms of the TKE budget were calculated by filtering the data to the roll frequency. The results obtained from the UW and NCAR King Air flights at different levels within the CBL are given in Table 2. For the unorganized convection case, buoyancy dominated at both levels observed. For the roll cases, however, buoyancy and shear were comparable at low levels ($0.1z_i$) while buoyancy dominated at $0.4z_i$ and above.

These aircraft observations imply that both thermal and shear instability acted to sustain the rolls, as previously suggested. In addition, these results suggest that the low-level shear was more important than the CBL shear in sustaining rolls since the shear term was important near the surface and decreased with height for the roll cases. Similar results of the shear production term being important only at low levels were obtained by Pennell and LeMone (1974). Thus, shear seemed to have significant influence in determining roll events, even though rolls occurred with CBL shear values as low as 2×10^{-3} s^{-1} (see Fig. 9). *Low-level* shear values may have been much larger for the roll cases than for the nonroll cases. Kristovich (1993) also suggested that the low-level shear was important in the production of rolls. Unfortunately reliable measurements of the shear in the lowest 200 m were unavailable during CaPE. Due to the set-up of the model, the question of the importance of low-level versus CBL shear could not be addressed with the simulations either. As discussed in the methodology section, the CBL shear is generally maintained in the atmosphere by external forcing, such as large-scale pressure gradients or momentum advection. Since these effects were not included in the model, it was difficult to maintain a CBL shear.

6. Roll characteristics

a. Aspect ratio

1) OBSERVATIONS

The roll wavelength, measured from updraft to updraft in the cross-roll direction, has been theoretically and observationally linked to the depth of the CBL (e.g.,

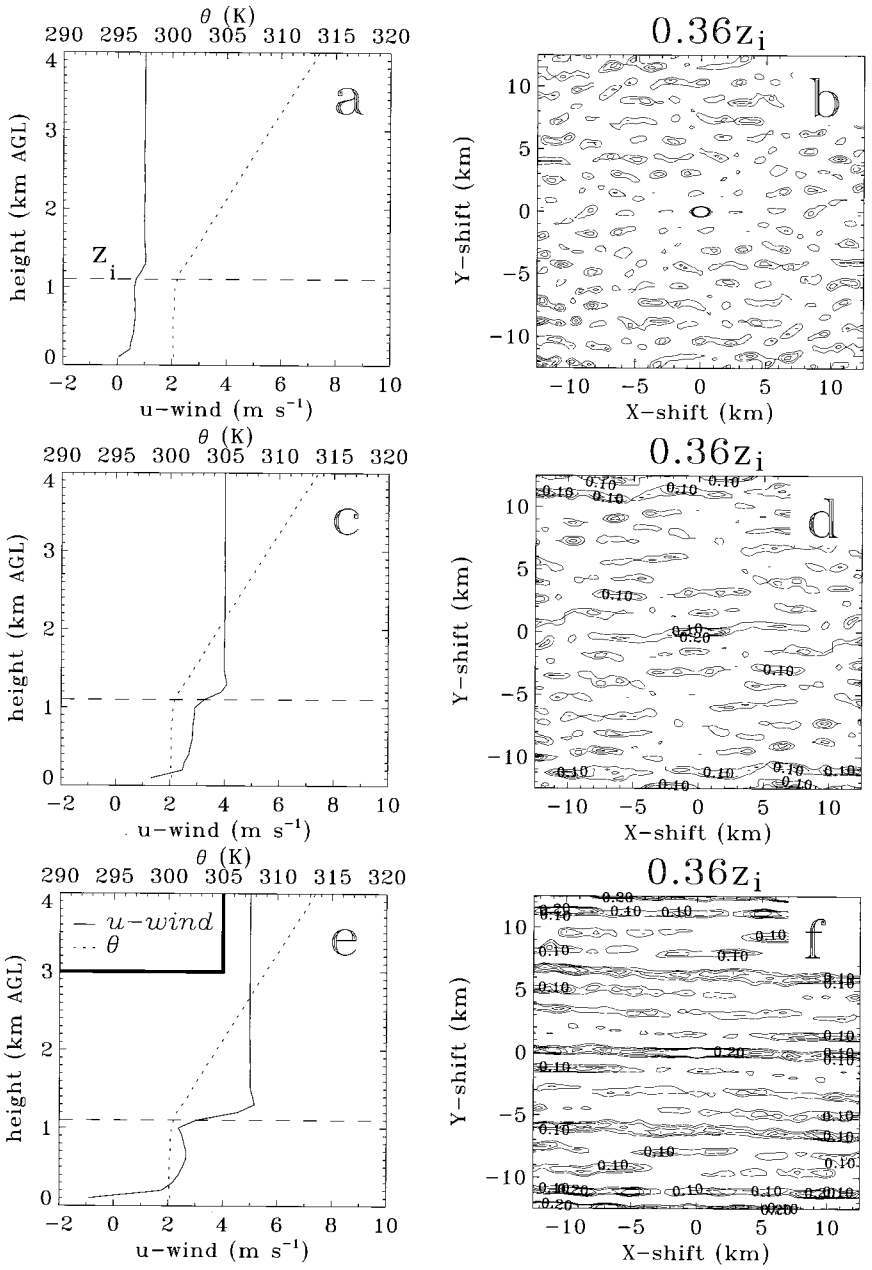

FIG. 13. Model output at 120 min comparing various wind speed profiles: (a,b) 2 m s^{-1}, (c,d) 5 m s^{-1}, and (e,f) 10 m s^{-1}. The left column shows the potential temperature (K; dashed line) and meridional wind component (m s^{-1}; solid line) profiles. The top of the CBL is indicated by the horizontal dashed line. The right column shows the corresponding results from the autocorrelation routine performed upon the vertical velocity field. The height at which the routine was performed is indicated at the top of (b), (d), and (f).

Lilly 1966; Kuettner 1971; LeMone 1973). Figure 17 shows a plot of CBL depth versus roll wavelength for CaPE events. Only the points with HARs greater than 6 (i.e., the roll cases) have been plotted. The linear correlation coefficient between the two variables is 0.84. Although the best-fit line is different from Kuettner's (1971) results, the average aspect ratio (5.7) falls within the range of previous work (e.g., LeMone 1973). The three outliers from Kuettner's curve with wavelengths greater than 4 all exhibited HARs greater than 8 and were therefore not marginal cases of roll occurrences.

The aspect ratio was then compared with various measurements to ascertain the parameters influencing its magnitude. Previous work suggested that a relationship may be found between the aspect ratio and the CBL wind shear (e.g., Melfi et al. 1985; Asai 1970a). The

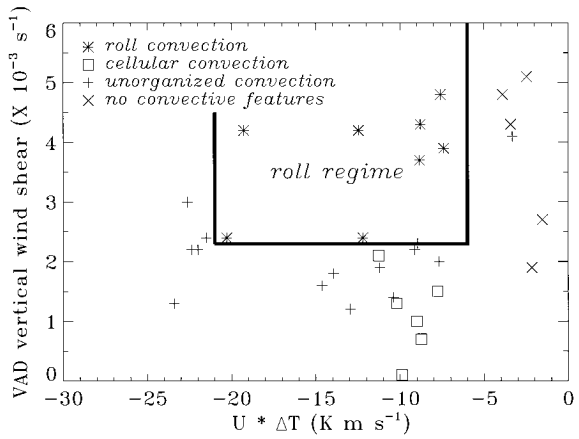

FIG. 14. Sensible heat flux (K m s^{-1}) vs CBL wind shear ($\times 10^{-3}$ s^{-1}) partitioned into radar-determined convective modes. Observed roll regime is indicated by a box.

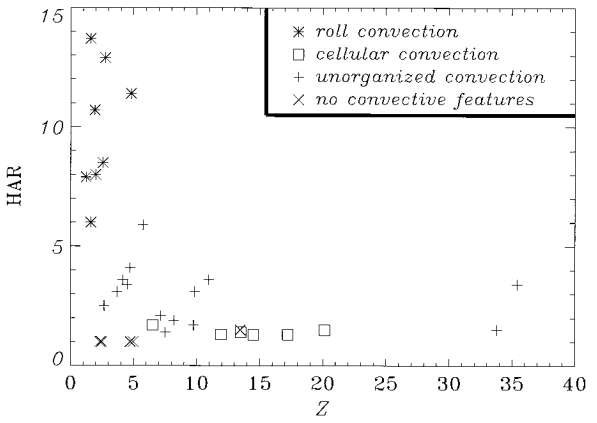

FIG. 16. Convective instability vs HAR partitioned into the radar-determined convective modes.

linear correlation coefficient was insignificant with this CaPE dataset ($r = -0.26$; not shown). Faller (1965) and Shirer (1986) speculated that the roll wavelength is governed by the wind speed by conducting laboratory and modeling studies, respectively. It was suspected that longer wavelength rolls occurred with faster wind speeds. This was not apparent in the plot of mean CBL wind speed versus wavelength ($r = -0.03$; not shown). The theory by Clark et al. (1986) was also addressed with the observations. They found that internal gravity waves could form in the troposphere if there was significant shear atop the CBL. Through a feedback mechanism, these waves may then influence the roll aspect ratio within the CBL. As shown in Fig. 10 there was consistently little shear throughout the lowest 3 km so their proposed gravity wave/CBL interaction was likely minimal. Theory (Kuo 1963) and previous observations (Kelly 1984) suggested that the aspect ratio is related to the CBL stability. Figure 18 shows that the CaPE dataset exhibited a correlation between aspect ratio and Z, or the CBL stability parameter. That is, the greater the convective instability, the greater the aspect ratio. When the outliers apparent in Fig. 17 were normalized by z_i, they became important in determining the influence of Z in modifying the aspect ratio.

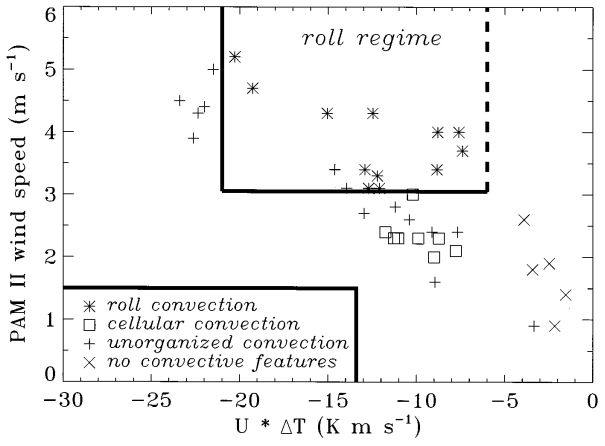

FIG. 15. Sensible heat flux (K m s^{-1}) vs PAM wind speed (m s^{-1}) partitioned into radar-determined convective modes. Observed roll regime is indicated by a box. The right border is dashed due to lack of data points to verify its existence.

2) MODEL SIMULATIONS

In an attempt to verify the observational results the numerical model was again utilized in sensitivity studies. All three of the simulations shown in Fig. 19 were performed with the same input parameters except for varying CBL depths. All of the $-z_i/L$ values were less than 10 and linear convection was produced in all three simulations. It is apparent that the simulation with a deeper CBL depth (Fig. 19f) produced longer-wavelength rolls than the simulation with a shallower CBL depth (Fig. 19b).

The comparison of sensible heat fluxes was shown in Fig. 8. Although the linearity of the convection diminished as the heat flux increased, the change in aspect ratio was examined. For the case with low sensible heat flux (Fig. 8b; $-z_i/L = 5.6$) the aspect ratio was 1.45.

TABLE 2. Comparison of buoyancy (B) and shear (S) terms of the TKE budget for unorganized and roll convection cases. All terms were filtered to the range of roll frequencies.

	Height (z/z_i)	B ($\times 10^{-5}$ m^2 s^{-3})	S ($\times 10^{-5}$ m^2 s^{-3})
27 July 1991 Unorganized convection	0.1	85	40
	0.5	105	17
2 August 1991 Rolls	0.1	60	58
	0.5	62	30
	0.7	47	14
6 August 1991 Rolls	0.1	63	44
	0.4	109	18
	0.6	44	6

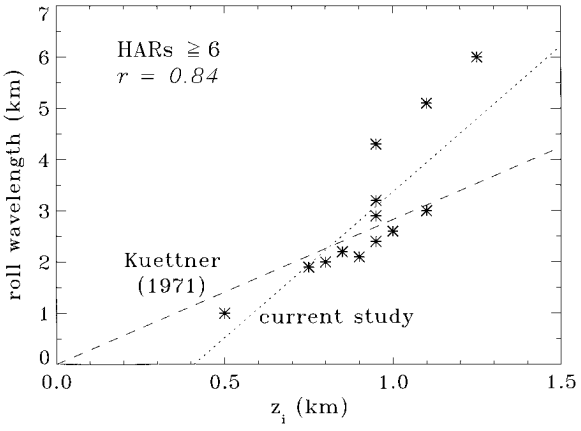

FIG. 17. CBL depth (km) vs wavelength (km) for roll cases. Kuettner's (1971) theoretically and observationally determined relationship is indicated by a dashed line. The linear regression for the current dataset is shown by the dotted line.

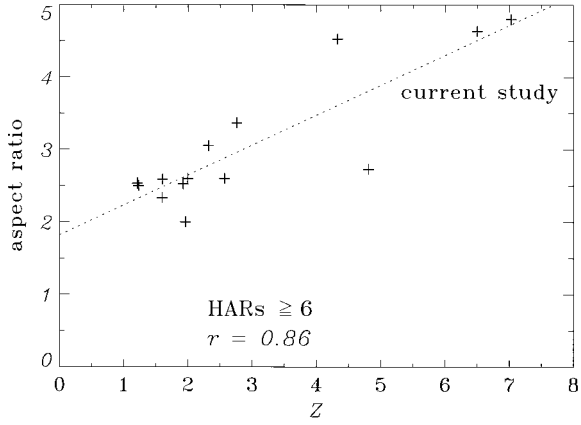

FIG. 18. Convective instability vs aspect ratio for the roll cases. The linear regression for the current dataset is shown by the dotted line.

The simulation with a larger CBL instability (Fig. 8d; $-z_i/L = 56.7$) produced a greater aspect ratio of 1.6. The final simulation (Fig. 8f; $-z_i/L = 129.4$) resulted in an aspect ratio of 1.75.

Results of both the numerical simulations and the observations suggested that the roll wavelength was related to the CBL depth. When the aspect ratio was obtained by normalizing the wavelength by the CBL depth, the observations and simulations both implied that larger aspect ratios were produced within more convectively unstable CBLs.

b. Orientation

Shirer's (1980) linear model can be used to predict the orientation and aspect ratio of two-dimensional modes that are unstable. Shirer (1980) defines a critical Rayleigh number [his Eq. (3.11)] for the development of rolls that is the sum of two terms: one depending on the aspect ratio and the other on the wind curvature in the cross-roll direction. As the roll orientation varies, the wind curvature in the cross-roll direction and hence the second term varies, vanishing at a certain orientation, which is then the orientation of the most unstable mode.

This calculation has been performed for two roll cases and reasonable agreement between the predicted and observed orientation and aspect ratios was found. For the case on 2 August at 1530 UTC, the orientation of the most unstable mode, according to Shirer's (1980) model, is 170° which is to be compared with an observed orientation of 182°. The range of aspect ratios that are unstable for a given Rayleigh number has also been calculated. The Rayleigh number on this day was estimated to be between 3×10^2 and 3×10^4 [using a 0.1° change in potential temperature across the boundary layer depth of 950 m and assuming an eddy viscosity μ and thermometric conductivity κ between 10 and 1 $m^2\ s^{-1}$ (Stull 1988)]. At the most unstable orientation, the aspect ratio of unstable modes, according to Shirer's (1980) theory, varies between 0.5 and 34 for $Ra = 3 \times 10^2$ and 0.15 and 350 for $Ra = 3 \times 10^4$. Both ranges adequately cover the observed aspect ratio of 3.4. For the conditions at 1700 UTC 10 August, the most unstable orientation is 279° (cf. an observed orientation of 258°) and the range of unstable aspect ratios varies between 0.3 and 80 for $Ra = 1.7 \times 10^3$ and 0.1 and 200 for $Ra = 1.7 \times 10^5$ (cf. an observed aspect ratio of 4.1).

Brown's (1972) inflection-point instability theory using an Ekman spiral predicts that roll orientation should be dependent upon the geostrophic wind within the CBL capping inversion. This theory was examined in this study by using the wind at a height of 1.1 times the depth of the CBL (Fig. 20). There was a positive correlation coefficient of 0.99 although the orientation did not seem to vary with the stability of the CBL, as predicted by Brown (1972; not shown).

Other studies (e.g., Ferrare 1991) have suggested that roll orientation is governed by the CBL vertical wind shear direction. This was also true with the CaPE dataset ($r = 0.97$; Fig. 21). In addition, there was a high correlation between roll orientation and the mean CBL wind direction ($r = 0.99$; Fig. 20), as well as with the PAM wind direction ($r = 0.98$; Fig. 21).

The reason that the roll orientation was well correlated with all of these wind directions was that the wind directions were all correlated with one another. There was not much directional shear in the wind profiles during the CaPE project (see VAD profiles in Fig. 10). Therefore, it was not possible to determine which of the wind direction measurements was dominant in governing the roll orientation with this dataset. This issue was not addressed with the numerical model since there were no observations from CaPE with directional shear with which to compare the simulated results.

7. Summary and conclusions

Although the topic of rolls has been extensively examined in the past, the present study profited from the

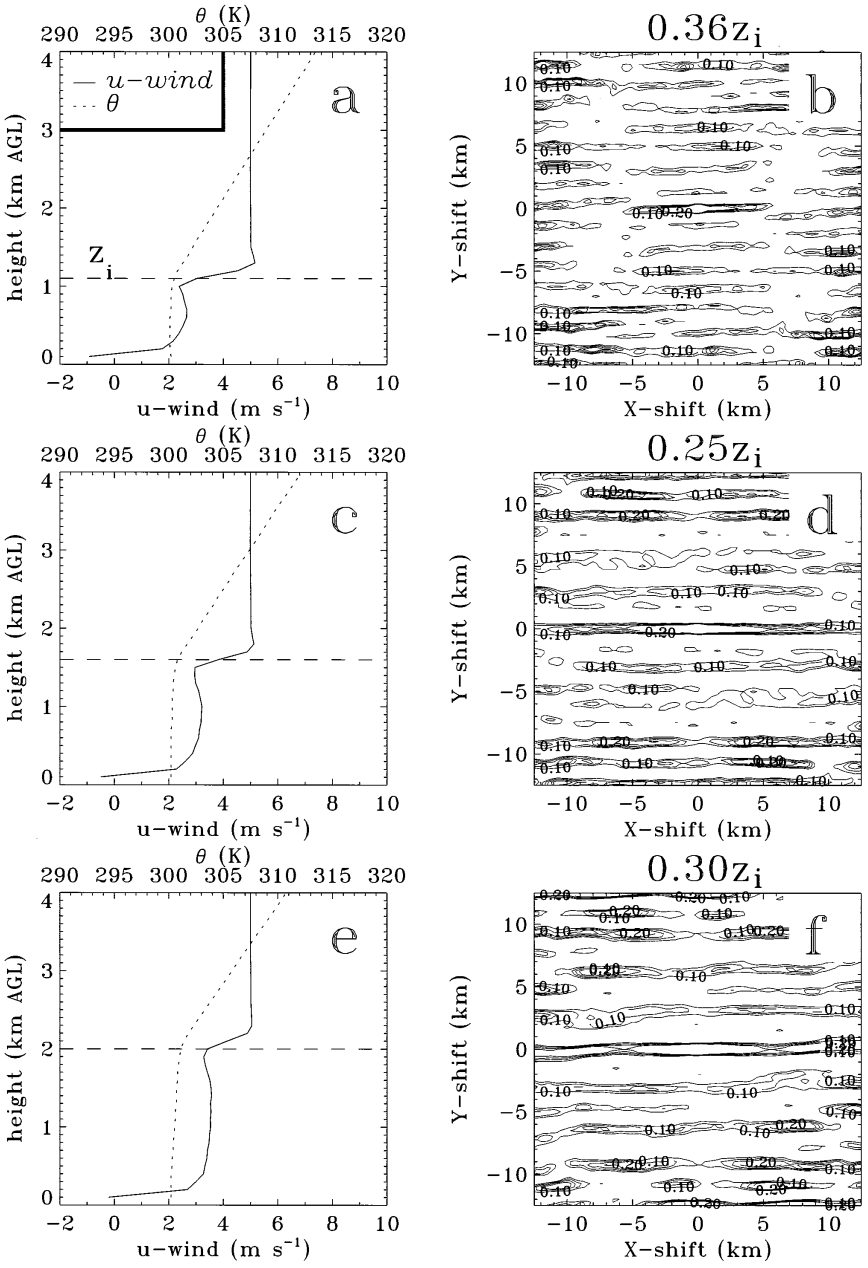

FIG. 19. Model results at 120 min comparing roll wavelength with various CBL depths: (a,b) 1.1 km, (c,d) 1.6 km, and (e,f) 2.0 km. The left column shows the potential temperature (K; dashed line) and meridional wind component (m s^{-1}; solid line) profiles. The top of the CBL is indicated by the horizontal dashed line. The right column shows the corresponding results of the autocorrelation routine performed upon the vertical velocity field. The height at which the routine was performed is indicated at the top of (b), (d), and (f).

collection of pertinent data within an extensive field program and employed unique approaches in diagnosis. The unique features of this study are as follows:

- An objective method of defining rolls and measuring their wavelength and orientation was utilized. This was accomplished by applying a spatial autocorrelation routine to the radar reflectivity field.
- Numerous observational platforms (i.e., radar, satellite, PAM stations, soundings, aircraft data, and cloud photography) provided the capability of differentiating among the environmental conditions defining the various convective modes and determining roll characteristics.
- The plethora of CaPE observations under varying en-

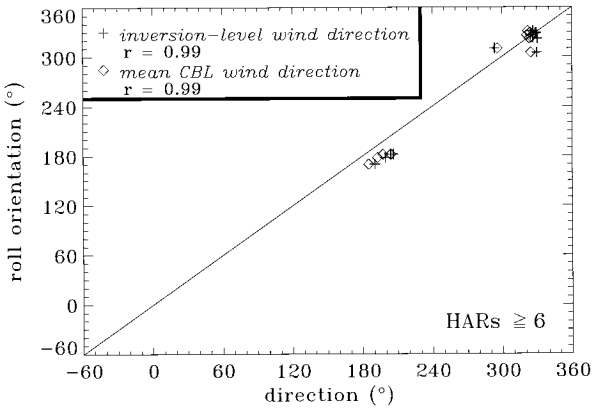

FIG. 20. Inversion-level wind direction (°; crosses) and mean CBL wind direction (°; diamonds) vs roll orientation (°) for the roll cases. The one-to-one line is shown for reference.

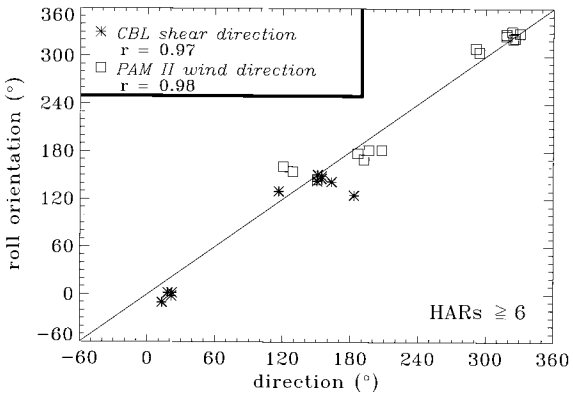

FIG. 21. CBL shear direction (°; stars) and mean PAM II wind direction (°; boxes) vs roll orientation (°) for the roll cases. The one-to-one line is shown for reference.

vironmental conditions and the numerical model, which allowed for the systematic exploration of a larger parameter space, were useful in substantiating the generality of the results.

a. Results

In agreement with some previous work, there appeared to be a minimum wind speed of 5.5 m s^{-1} throughout the CBL (or 3 m s^{-1} at the 10-m PAM height) necessary for roll existence. The minimum wind speed criterion was corroborated in the numerical simulations. Unlike some of the past work, however, there were observations of rolls within very low CBL shear conditions (2×10^{-3} s^{-1}). Although a high surface-layer shear value was necessary to produce rolls in the model, there was also very little shear across the entire CBL in the simulations. It was apparent that directional shear was not required for roll occurrences. There was virtually no directional shear within the CBL during CaPE nor was there any in the roll simulations.

The PAM wind measurements, VAD profiles, and the calculations of the TKE budget suggested that the low-level shear was more important than the shear across the entire CBL in sustaining rolls. This could not be addressed with direct observations since there were no wind measurements between 10 m (i.e., the PAM wind measurement) and approximately 200 m (i.e., the lowest reliable VAD wind measurement). The numerical model could not provide insight on this issue due to its inability to maintain a given CBL shear.

The CaPE observations suggested that rolls are the preferred convective mode within a certain heat flux/wind regime. Several cautions should be noted in relation to the significance of heat flux in this analysis: 1) a simplification was required in calculating Z as a proxy for $-z_i/L$ without actual measurements of surface heat and momentum fluxes; 2) it is possible that rolls were occurring at low heat flux values (i.e., early in the morning) but were not resolved by the radar. The importance of both buoyancy and shear was corroborated by aircraft flux measurements of the terms of the TKE budget. Although the model results also suggested a minimum wind speed for roll occurrences, they suggested only a maximum heat flux limit for rolls but not a necessary minimum.

The observations suggested that the roll wavelength was proportional to the CBL depth and that the aspect ratio increased as the CBL instability, as defined by Z, increased. The model simulations were consistent with both of these results.

Finally the roll orientation was highly correlated with all wind directions: the PAM wind, the mean CBL wind, the CBL wind shear and the stable-layer wind directions. This is due to the fact that there was little directional shear with height.

b. Future work

Although this dataset was more comprehensive than many previous studies, all of the findings should be reexamined with the use of additional carefully selected observational platforms. Given the limitations of accurately measuring low-level shear, surface fluxes, and CBL depth in this study, another project was conducted in east-central Florida during the summer of 1995. The goal was to deploy facilities necessary to address many of the issues presented herein. These facilities included three prototype flux-PAM (PAM III) stations to ascertain the surface flux values (Militzer et al. 1995; Horst and Oncley 1995), the UW King Air to examine the representativeness of the flux-PAM stations, an integrated sounding system (ISS) and a tethersonde instrument to measure CBL depth and low-level shear.

Analyses of the evolution of boundary layer convective features are being performed. The Small Cumulus Microphysical Study dataset includes observations from all platforms from the preroll environment to roll conditions to unorganized convection to quiescent condi-

tions. As suggested with the CaPE dataset and some of the previous work, the surface-layer heat and momentum fluxes defining the convective instability within the CBL are being examined as the forcing mechanisms influencing the evolution.

Acknowledgments. Several discussions with and detailed reviews by P. LeMone (NCAR), T. Horst (NCAR), and D. Stensrud (NOAA/NSSL) were invaluable. Help from J. Pinto (CU-Boulder) on computer code development and figure preparation is greatly appreciated. R. Kelly provided helpful insight on Shirer's model. All of the radar, sounding, and surface station data were obtained from B. Rilling (NCAR). S. Williams (UCAR) provided the satellite imagery. The software package REORDER, written by D. Oye (NCAR) and M. Case (NCAR), was used to interpolate the radar data onto a Cartesian grid. The aircraft analysis package XANADU, developed in NCAR/MMM, was used to obtain aircraft flux measurements. Special gratitude is bestowed upon the NCAR/ATD field support personnel who collected the data during CaPE. The careful review by an anonymous reviewer is appreciated. Research results presented herein were partially supported by NSF under Grants ATM 9221951 and ATM 9422499.

REFERENCES

Angell, J. K., D. H. Pack, and C. R. Dickson, 1968: A Lagrangian study of helical circulations in the planetary boundary layer. *J. Atmos. Sci.,* **25,** 707–717.

Asai, T., 1970a: Stability of a plane parallel flow with variable vertical shear and unstable stratification. *J. Meteor. Soc. Japan,* **48,** 129–139.

——, 1970b: Three-dimensional features of thermal convection in a plane Couette flow. *J. Meteor. Soc. Japan,* **48,** 18–29.

——, 1972: Thermal instability of a shear flow turning the direction with height. *J. Meteor. Soc. Japan,* **50,** 525–532.

Atlas, D., B. Walter, S.-H. Chou, and P. J. Sheu, 1986: The structure of the unstable marine boundary layer viewed by lidar and aircraft observations. *J. Atmos. Sci.,* **43,** 1301–1318.

Balaji, V., and T. L. Clark, 1988: Scale selection in locally forced convective fields and the initiation of deep cumulus. *J. Atmos. Sci.,* **45,** 3188–3211.

Berger, M. I., and R. J. Doviak: 1979: An analysis of the clear air planetary boundary layer wind synthesized from NSSL's dual-Doppler radar data. NOAA Tech. Memo. ERL NSSL-87, 59 pp. [Available from National Technical Information Service, U. S. Department of Commerce, Springfield, VA 22161.]

Brown, R. A., 1970: A secondary flow model of the planetary boundary layer. *J. Atmos. Sci.,* **27,** 742–757.

——, 1972: On the inflection point instability of a stratified Ekman boundary layer. *J. Atmos. Sci.,* **29,** 851–859.

——, 1980: Longitudinal instabilities and secondary flows in the planetary boundary layer: A review. *Rev. Geophys. Space Phys.,* **18,** 683–697.

Brümmer, B., 1985: Structure, dynamics, and energetics of boundary layer rolls from KonTur aircraft observations. *Contrib. Atmos. Phys.,* **58,** 237–254.

Christian, T. W., 1987: A comparative study of the relationship between radar reflectivities, Doppler velocities, and clouds associated with horizontal convective rolls. M.S. thesis, Department of Atmospheric Sciences, University of California, Los Angeles, 94 pp. [Available from University of California, Los Angeles, 405 Hilgard Ave., Los Angeles, CA 90095-1565.]

——, and R. M. Wakimoto: 1989: The relationship between radar reflectivities and clouds associated with horizontal roll convection on 8 August 1982. *Mon. Wea. Rev.,* **117,** 1530–1544.

Clark, T. L., 1977: A small scale numerical model using a terrain following coordinate transformation. *J. Comput. Phys.,* **24,** 186–215.

——, and R. D. Farley, 1984: Severe downslope windstorm calculations in two and three spatial dimensions using anelastic interactive grid nesting: A possible mechanism for gustiness. *J. Atmos. Sci.,* **41,** 329–350.

——, T. Hauf, and J. P. Kuettner, 1986: Convectively forced internal gravity waves: Results from two-dimensional numerical experiments. *Quart. J. Roy. Meteor. Soc.,* **112,** 899–925.

Cressman, G. P., 1959: An operational objective analysis scheme. *Mon. Wea. Rev.,* **87,** 367–374.

Deardorff, J. W., 1972: Numerical investigation of neutral and unstable planetary boundary layers. *J. Atmos. Sci.,* **29,** 91–115.

Doviak, R. J., and M. Berger, 1980: Turbulence and waves in the optically clear planetary boundary layer resolved by dual-Doppler radars. *Radio Sci.,* **15,** 297–317.

Faller, A. J., 1963: An experimental study of the instability of the laminar Ekman boundary layer. *J. Fluid Mech.,* **15,** 560–576.

——, 1965: Large eddies in the atmospheric boundary layer and their possible role in the formation of cloud rows. *J. Atmos. Sci.,* **22,** 176–184.

Fankhauser, J. C., C. J. Biter, C. G. Mohr, and R. L. Vaughan, 1985: Objective analysis of constant altitude aircraft measurements in thunderstorm inflow regions. *J. Atmos. Oceanic Technol.,* **2,** 157–170.

Ferrare, R. A., J. L. Schols, E. W. Eloranta, and R. Coulter, 1991: Lidar observations of banded convection during BLX83. *J. Appl. Meteor.,* **30,** 312–326.

Grossman, R. L., 1982: An analysis of vertical velocity spectra obtained in the BOMEX fair-weather, trade-wind boundary layer. *Bound.-Layer Meteor.,* **23,** 323–357.

Hauf, T., and T. L. Clark, 1989: Three-dimensional numerical experiments of convectively forced internal gravity waves. *Quart. J. Roy. Meteor. Soc.,* **115,** 309–333.

Hildebrand, P. H., 1980: Multiple-Doppler radar observations of PBL structure. Preprints, *19th Conf. on Radar Meteorology,* Miami, FL, Amer. Meteor. Soc., 67–70.

Horst, T. W., and S. P. Oncley, 1995: Flux-PAM measurement of scalar fluxes using cospectral similarity. Preprints, *Ninth Symp. on Meteorological Observations and Instrumentation,* Charlotte, NC, Amer. Meteor. Soc. 495–500.

Kaimal, J. C., and Coauthors, 1982: Estimating the depth of the daytime convective boundary layer. *J. Appl. Meteor.,* **21,** 1123–1129.

Kelly, R. D., 1982: A single Doppler radar study of horizontal-roll convection in a lake-effect snow storm. *J. Atmos. Sci.,* **39,** 1521–1531.

——, 1984: Horizontal roll and boundary-layer interrelationships observed over Lake Michigan. *J. Atmos. Sci.,* **41,** 1816–1826.

Kessinger, C. J., 1988: *Operation and Data Summary for the Convection INitiation and Downburst Experiment (CINDE) Held Near Denver, Colorado from 22 June to 7 August 1987.* NCAR, 131 pp.

Kessler, E., III, and J. A. Russo Jr., 1963: Statistical properties of weather radar echoes. Preprints, *Proc. of 10th Weather Radar Conf.,* Washington, DC, Amer. Meteor. Soc., 25–33.

Kristovich, D. A. R., 1993: Mean circulations of boundary-layer rolls in lake-effect snow storms. *Bound.-Layer Meteor.,* **63,** 293–315.

Kuettner, J. P., 1959: The band structure of the atmosphere. *Tellus,* **2,** 267–294.

——, 1971: Cloud bands in the earth's atmosphere. *Tellus,* **23,** 404–425.

Kuo, H. L., 1963: Perturbations of plane Couette flow in stratified fluid and origin of cloud streets. *Phys. Fluids,* **6,** 195–211.

LeMone, M. A., 1973: The structure and dynamics of horizontal roll vortices in the planetary boundary layer. *J. Atmos. Sci.,* **30,** 1077–1091.

Lilly, D. K., 1966: On the instability of Ekman boundary flow. *J. Atmos. Sci.,* **23,** 481–494.

Malkus, J. S., and H. Riehl, 1964: Cloud structure and distributions over the tropical Pacific Ocean. *Tellus,* **16,** 275–287.

Mason, P. J., and R. I. Sykes, 1982: A two-dimensional numerical study of horizontal roll vortices in an inversion capped planetary boundary layer. *Quart. J. Roy. Meteor. Soc.,* **108,** 801–823.

Matejka, T., and R. C. Srivastava, 1991: An improved version of the extended velocity-azimuth display analysis of single-Doppler radar data. *J. Atmos. Oceanic Technol.,* **8,** 453–466.

Melfi, S. H., J. D. Spinhirne, S.-H. Chou, and S. P. Palm, 1985: Lidar observations of vertically organized convection in the planetary boundary layer over the ocean. *J. Appl. Meteor.,* **24,** 806–821.

Militzer, J. M., M. C. Michaelis, S. R. Semmer, K. S. Norris, T. W. Horst, S. P. Oncley, A. C. Delany, and F. V. Brock, 1995: Development of the prototype PAM III/flux-PAM surface meteorological station. Preprints, *Ninth Symp. on Meteorological Observations and Instrumentation,* Charlotte, NC, Amer. Meteor. Soc., 490–494.

Miura, Y., 1986: Aspect ratios of longitudinal rolls and convection cells observed during cold air outbreaks. *J. Atmos. Sci.,* **43,** 29–39.

Moeng, C.-H., and P. P. Sullivan, 1994: A comparison of shear- and buoyancy-driven planetary boundary layer flows. *J. Atmos. Sci.,* **51,** 999–1022.

Oye, R., and R. E. Carbone, 1981: Interactive Doppler editing software. Preprints, *20th Conf. on Radar Meteorology,* Boston, MA, Amer. Meteor. Soc., 683–689.

Pennell, W. T., and M. A. LeMone, 1974: An experimental study of turbulence structure in the fair-weather trade wind boundary layer. *J. Atmos. Sci.,* **31,** 1308–1323.

Rabin, R. M., R. J. Doviak, and A. Sundara-Rajan, 1982: Doppler radar observations of momentum flux in a cloudless convective layer with rolls. *J. Atmos. Sci.,* **39,** 851–863.

Rayleigh, O. M., 1916: On convection currents in a horizontal layer of fluid, when the higher temperature is on the under side. *Philos. Mag. Ser.,* **6,** 529–546.

Reinking, R. F., R. J. Doviak, and R. O. Gilmer, 1981: Clear-air roll vortices and turbulent motions as detected with an airborne gust probe and dual-Doppler radar. *J. Appl. Meteor.,* **20,** 678–685.

Rothermel, J., and E. M. Agee, 1980: Aircraft investigation of mesoscale cellular convection during AMTEX 75. *J. Atmos. Sci.,* **37,** 1027–1040.

Shirer, H. N., 1980: Bifurcation and stability in a model of moist convection in a shearing environment. *J. Atmos. Sci.,* **37,** 1586–1602.

——, 1986: On cloud street development in three dimensions: Parallel and Rayleigh instabilities. *Contrib. Atmos. Phys.,* **59,** 126–149.

Sommeria, G., and M. A. LeMone, 1978: Direct testing of a three-dimensional model of the planetary boundary layer against experimental data. *J. Atmos. Sci.,* **35,** 25–39.

Stensrud, D. J., and H. N. Shirer, 1988: Development of boundary layer rolls from dynamic instabilities. *J. Atmos. Sci.,* **45,** 1007–1019.

Stull, R. B., 1988: *An Introduction to Boundary Layer Meteorology.* Kluwer Academic Publishers, 666 pp.

Sykes, R. I., and D. S. Henn, 1989: Large-eddy simulation of turbulent sheared convection. *J. Atmos. Sci.,* **46,** 1106–1118.

Wakimoto, R. M., and N. T. Atkins, 1994: Observations of the sea-breeze front during CaPE. Part I: Single-Doppler, satellite, and cloud photogrammetry analysis. *Mon. Wea. Rev.,* **122,** 1092–1114.

Walter, B. A., and J. E. Overland, 1984: Observations of longitudinal rolls in a near neutral atmosphere. *Mon. Wea. Rev.,* **112,** 200–208.

Weckwerth, T. M., 1995: *A Study of Horizontal Convective Rolls Occurring within Clear-Air Convective Boundary Layers.* Cooperative thesis 160, Department of Atmospheric Sciences, University of California, Los Angeles and National Center for Atmospheric Research, 179 pp. [Available from University of California, Los Angeles, 405 Hilgard Ave., Los Angeles, CA 90095-1565.]

Wilczak, J. M., and J. A. Businger, 1983: Thermally indirect motions in the convective atmospheric boundary layer. *J. Atmos. Sci.,* **40,** 343–358.

Wilson, J. W., T. M. Weckwerth, J. Vivekanandan, R. M. Wakimoto, and R. W. Russell, 1994: Boundary layer clear-air radar echoes: Origin of echoes and accuracy of derived winds. *J. Atmos. Oceanic Technol.,* **11,** 1184–1206.

Woodcock, A. H., 1942: Soaring over the open sea. *Sci. Mon.,* **55,** 226–232.